Tribology International 173 (2022) 107593

Contents lists available at ScienceDirect

Tribology International

journal homepage: www.elsevier.com/locate/triboint

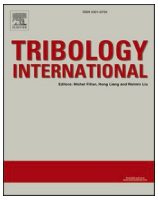

A novel method to evaluate the journal bearing forces with application to flexible rotor model

Hussein Sayed [a], T.A. El-Sayed [a,b,c,*]

[a] Department of Mechanical Design, Faculty of Engineering, Mataria, Helwan University, P.O. Box 11718, Helmeiat-Elzaton, Cairo, Egypt
[b] Centre for Applied Dynamics Research, School of Engineering, University of Aberdeen, Aberdeen AB24 3UE, UK
[c] School of Engineering, University of Hertfordshire Hosted by Global Academic Foundation, Cairo, Egypt

ARTICLE INFO

Keywords:
Rotor-bearing system
Journal bearing
Reynolds equation
Polynomial fitting
Hopf bifurcation
Numerical continuation

ABSTRACT

In this work, a novel method to evaluate the nonlinear bearing forces is introduced. The method depends on using polynomial surface fitting to evaluate the bearing forces as a function of the journal center position. Then, these forces are used to investigate the stability and bifurcations of an elastic rotor-bearing model. The Hopf bifurcation analysis and limit cycle continuation are investigated using the proposed analysis for obtaining the bearing forces for un-grooved bearing with $L/D = 0.5$. The stability results are compared with short bearing approximation at several shaft flexibilities. In addition, the present obtained threshold speed is compared with that computed using bearing coefficients method. The present method time response results are compared with the numerical solution of Reynolds equation and a good agreement is recorded.

1. Introduction

Bearings are one of the main components of dynamical systems. There are two main categories of bearings which are rolling element bearings and journal bearings. Each type has its advantages and disadvantages. For example, rolling element bearings have the advantage of less axial space, combined loading conditions, less maintenance and gradual failure. However, journal bearing has advantage in high load-carrying capacity, low noise and can operate at very high speeds [1]. The industries which require high speed and high power, such as gas turbines and turbochargers motivate the research in the dynamics of journal bearings, and this is the main topic of the current paper.

To investigate the dynamics of journal bearing, it is important to evaluate the nonlinear dynamic forces at the bearing. The fluid film pressure distribution inside the journal bearing can be described by Reynolds equation [2]. This generalized Reynolds equation can be simplified in case of short bearings or long bearings. For these cases, analytical solutions for the bearing forces are available, see for example [3,4] for short bearings [5–8] and [9,10] for long bearings. Direct solution of generalized Reynolds is important in case of finite length bearings (FLB), because in that case both short bearing and long bearing approximations are not valid. The analytical solution for bearing forces is challenging, see for example [11]. In that case, either numerical methods or approximate analytical methods are used to solve the problem [12,13]. The numerical methods include finite difference methods [14,15], finite element method [16,17], meshless method [14], etc. In rotor-bearing dynamical analysis, the journal bearing forces have to be evaluated at each time step. In case of finite bearings, the numerical solution of Reynolds equation is required and this process is computationally expensive especially if fine mesh is used. This motivates a lot of researchers to use approximate methods to evaluate the journal bearing forces in such cases.

Using bearing coefficients is one of the common methods used to evaluate the bearing forces based on the rotor displacement and velocity. First order bearing coefficient was introduced in the middle of the last century and it is currently used till now due to its simplicity, see for example [18–21]. The analysis based on first order bearing coefficients is accurate up to the rotor threshold speed or in other words until the speed at which Hopf bifurcations occurs [22,23]. Higher than this speed the first order approximation indicates the system become unstable while in reality this is not generally the case. Several authors reported stable operation higher than threshold speed [24,25]. Therefore, much research work considered the evaluation of journal bearing forces using higher order bearing stiffness and damping coefficients. For the second order bearing stiffness and damping coefficients, see [23,26,27] and for the higher order bearing stiffness and damping coefficients, see [22,28,29]. The analysis based on higher order bearing coefficient gives better

* Corresponding author at: Department of Mechanical Design, Faculty of Engineering, Mataria, Helwan University, P.O. Box 11718, Helmeiat-Elzaton, Cairo, Egypt.
E-mail addresses: husseinsayed2008@m-eng.helwan.edu.eg (H. Sayed), tamer.elsayed@abdn.ac.uk (T.A. El-Sayed).

https://doi.org/10.1016/j.triboint.2022.107593
Received 6 January 2022; Received in revised form 11 April 2022; Accepted 19 April 2022
Available online 26 April 2022

Nomenclature

c	the radial clearance [m]
C_{XX}, C_{YX}, C_{XY}, C_{YY}	the bearing damping coefficients
e	the eccentricity between the rotor center and the bearing center [m]
F_x, F_y	the forces resulted from the oil film pressure in x and y directions [N]
$\overline{F}_X$, $\overline{F}_Y$	dimensionless bearing forces components $\overline{F}_X = \frac{F_x}{W} = \frac{F_X}{W}$, $\overline{F}_Y = \frac{F_y}{W} = \frac{F_Y}{W}$
h	the oil film thickness [m]
H	the dimensionless oil film height $H = \frac{h}{c}$
k_s	the rotating shaft lateral stiffness [N/m]
K_S	dimensionless shaft stiffness $K_S = \frac{k_s \quad c}{W}$
m	the total mass of the disc and the shaft $m = m_d + 2m_j$ [kg]
m_d	disc mass and shaft around it [kg]
m_j	mass of the journal and shaft around it [kg]
$\overline{M}$	dimensionless mass $\overline{M} = \frac{m \quad c \quad \Omega^2}{W}$
$\overline{M}_{th}$	threshold mass $\overline{M}_{th} = \frac{m \quad c \quad \Omega_{th}^2}{W}$
p	the oil film pressure [Pa]
P	the dimensionless pressure $P = \frac{p}{6\mu\Omega}\left(\frac{c}{R}\right)^2$
$P_P(X, Y)$	the dimensionless pressure at $\frac{\partial H}{\partial \tau} = 0$
$P_{X'}, P_{Y'}$	the dimensionless pressure gradients
r	the journal radius [m]
R	the bearing radius [m]
S	the Sommerfeld number $S = \frac{\mu\Omega r L}{\pi W}\left(\frac{r}{c}\right)^2$
t	the time [s]
W	the static applied load on the bearing [N]
$\overline{W}$	the dimensionless load for finite bearing $\overline{W} = \frac{L/D}{3\pi \quad S}$
x_d, y_d	the geometrical center for the rotating disc
x_j, y_j	the geometrical center for the journal mass
X_J, Y_J	the dimensionless position of the journal center
$X_J^{'}, Y_J^{'}, X_J^{''}, Y_J^{''}$	dimensionless velocities and accelerations of Journal center.
z	the coordinate in the axial direction [m]
Z	the dimensionless axial location $Z = \frac{z}{R}$
ε	eccentricity ratio $\varepsilon = e/c$
θ	the attitude angle [rad]
μ	the oil film viscosity [Pa s]
τ	the dimensionless time $\tau = \Omega t$
ϕ	the circumference coordinate [rad]
Ω	the angular velocity of the rotor [rad/s]

approximation than the analysis based on first order approximation, in terms of dynamic response and stability analysis [22]. However, in certain conditions higher than the threshold speed, there is a deviation between the analysis based on nonlinear stiffness and damping bearing coefficients and the analysis based on direct solution of Reynolds equation [20,29].

There are several attempts to evaluate an approximate form for Reynolds equation in case of finite length bearing $0.5 \leq L/D \leq 2$ which enable the analytical solution of this equation [13,30]. Fedor [30] introduced an approximate analytical solution for finite length journal bearing based on the complete oil solution of [31]. Barrett et al. [32] introduced a correction factor which modifies the nonlinear forces obtained from short bearing analysis. They showed that the analysis is valid up to L/D equals to 1.25. The disadvantage of this method is that it is only applicable to circular bearing without any grooves [33]. Hirani et al. [34] introduced a closed-form pressure distribution to finite bearing using a combination of short and long bearing approximation. Falkenhagen et al. [35] investigate the stability of finite journal bearing using approximate method and using direct solution of Reynolds equation using finite difference method (FDM). They showed that the response results based on the approximate are acceptable compared with that of FDM and 100 times faster. Bastani and de Queiroz [13] introduced a method for determining an approximate analytical form to the finite length journal bearing based on either short bearing approximation or long bearing approximation. The correction function is evaluated based on the comparison between the short or long bearing with numerical solution. Database method is another method that is used to evaluate the bearing nonlinear forces, see for example [36–38]. In this method,the oilfilm nonlinear forces are evaluated at several points in four-dimensional bearing domain to evaluate a database. Then, linear interpolation method is used to evaluate the force based on this database.This method is faster than the direct solution of Reynolds equation.

Miraskari et al. [23] investigated the response of flexible rotor-journal bearing system based on four approaches. These are, first order bearing coefficients, second order bearing coefficients, short bearing analysis and finite bearing using FDM. They investigated two different Sommerfeld number cases where the first case is located in supercritical bifurcation region and the second case is located in subcritical bifurcation region. Their results showed that below the supercritical bifurcation the results obtained from the four methods are matched together. Elsayed and Sayed [29] investigated the response of flexible rotor-bearing system using two cases the first is supercritical and the second is subcritical. They used four methods to evaluate the system response which are, first, second and third order bearing coefficient and direct solution of Reynolds equation using FDM. Their results show that the four methods produce the same results before the threshold speed limit. However, there is considerable deviations between these methods higher than the threshold speed. This deviation is more persistent in case of subcritical bifurcation regions.

Smolík et al. [39] investigated the stability of rotor-bearing system in which the bearing type is journal bearings. They used four approaches to evaluate the hydrodynamics forces which are infinitely short bearing (ISB) approximation, finite length journal bearing approximate solution based on short bearing analysis (ISCOR), finite difference method and finite element method. They concluded that ISCOR is not recommended in evaluating the system threshold stability. Chasalevris et al. [40] investigated. Stability and Hopf bifurcations in rotor-bearing-foundation systems of turbines and generators. They used Hopf bifurcation theory for investigating the rotor stability. Wang and Khonsari [41] investigated the effect of rotor stiffness on the bifurcation region of a flexible rotor. They also used Hopf bifurcation theory to investigate the rotor stability. In another publication [42], they investigated the bearing stability while considering turbulent effects on the bearings. Wang and Khonsari [43] introduced a method for Predicting of the stability envelope of rotor-bearing systems.

The previous literature shows the importance of finding an accurate close form solution to the problem of finite-length bearings, because such solution will inherently speed up the dynamical analysis solution and enables deeper understanding of the dynamical system. This motivates the authors of this paper to investigate a new method to approximate the nonlinear bearing forces in case of finite length bearings. After this introduction, the steps of the present analysis and the flexible rotor-bearing model are presented in the analytical section. Then, the verification results and the validity range of the present method are discussed in the results Section. Finally, the main findings of the present analysis are listed in the conclusion Section.

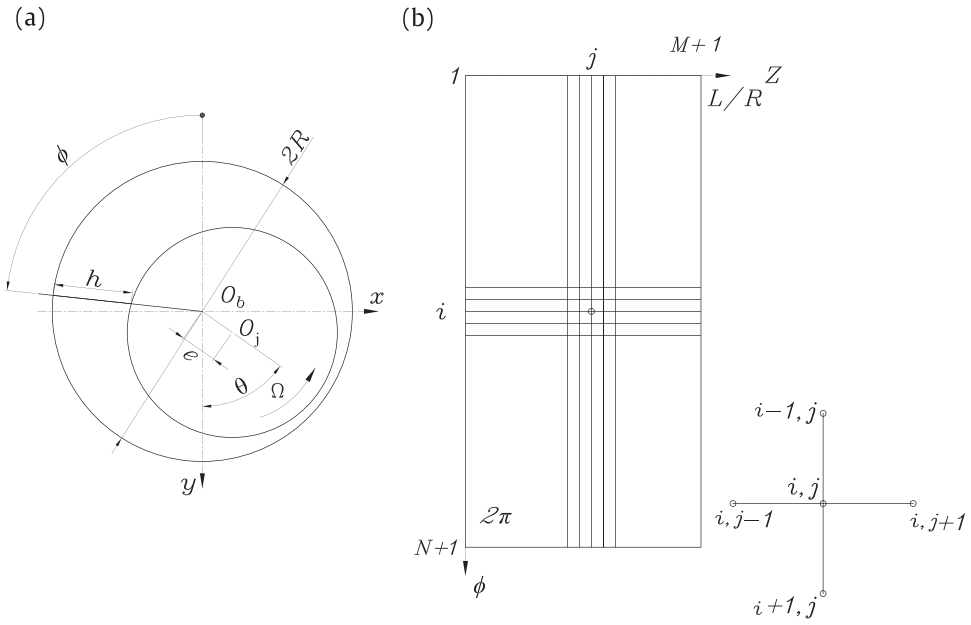

Fig. 1. Full circular journal bearing (a) schematic of the journal bearing coordinates (b) journal bearing mesh.

2. Analytical models

2.1. Proposed approximation of journal bearing model

The model used in this work is a full circular journal bearing as shown in Fig. 1-a. The pressure distribution of the oil film inside the journal bearing can be described by the differential Reynolds equation. To evaluate the bearing forces, this equation should be solved.

The bearing center is O_b and the journal center is O_j. The oil film thickness is h and it is a function of eccentricity e, the circumference coordinate ϕ measured from the vertical line and the attitude angle θ, see Eq. (3). The bearing radius is R, the journal radius is r and the difference between them is the radial clearance $c = R - r$. The angular velocity of the rotor is Ω.

Assuming that the lubricant is Newtonian, isoviscous and incompressible, the Reynolds equation which describes the oil film pressure can be written as

$$\frac{1}{r^2}\frac{\partial}{\partial\phi}\left(\frac{h^3}{12\mu}\frac{\partial p}{\partial\phi}\right)+\frac{\partial}{\partial z}\left(\frac{h^3}{12\mu}\frac{\partial p}{\partial z}\right)=\frac{\Omega}{2}\frac{\partial(h)}{\partial\phi}+\frac{\partial h}{\partial t}, \tag{1}$$

for which p, t, z are the pressure of the oil film, the time and the coordinate in the axial direction respectively, see Fig. 1b for axial coordinates. The oil film viscosity is represented by μ. The Reynolds equation Eq. (1) can be written in the dimensionless form as follows

$$\frac{\partial}{\partial\phi}\left(H^3\frac{\partial P}{\partial\phi}\right)+\frac{\partial}{\partial Z}\left(H^3\frac{\partial P}{\partial Z}\right)=\frac{\partial H}{\partial\phi}+2\frac{\partial H}{\partial\tau}, \tag{2}$$

where the dimensionless height is $H = \frac{h}{c}$, the dimensionless pressure $P = \frac{p}{6\mu\Omega}\left(\frac{c}{R}\right)^2$ and the dimensionless axial location is $Z = \frac{z}{R}$ as shown in Fig. 1-b. The dimensionless time is $\tau = \Omega t$.

The dimensionless height H and its derivative with dimensionless time $\frac{\partial H}{\partial\tau}$ can be written as

$$H = 1+\varepsilon\cos(\phi-\theta) = 1+X_J\sin\phi+Y_J\cos\phi, \tag{3}$$

$$\frac{\partial H}{\partial\tau} = X_J'\sin\phi+Y_J'\cos\phi, \tag{4}$$

for which X_J, Y_J are the dimensionless position of the journal center. $X_J' = \frac{\partial X_J}{\partial\tau}$ and $Y_J' = \frac{\partial Y_J}{\partial\tau}$ are the components of dimensionless velocity of journal center in x and y directions.

As shown in Eqs. (2)–(4), the pressure distribution inside the journal bearing is dependent on four parameters $P = f(X_J, Y_J, X_J', Y_J')$. The first two parameters are for the position of journal center X_J, Y_J and the remaining two parameters are for the velocity of journal center X_J', Y_J'. This pressure distribution can be approximated around the surface $P = f(X_J, Y_J, X_J' = 0, Y_J' = 0)$ by using Taylor expansion as

$$\begin{aligned}P\left(X_J,Y_J,X_J',Y_J'\right) &= P_P(X_J,Y_J)+\frac{\partial P\left(X_J,Y_J,X_J',Y_J'\right)}{\partial X_J'}X_J'+\frac{\partial P\left(X_J,Y_J,X_J',Y_J'\right)}{\partial Y_J'}Y_J'\\ &= P_P(X_J,Y_J)+P_{X'}(X_J,Y_J)X_J'+P_{Y'}(X_J,Y_J)Y_J',\end{aligned} \tag{5}$$

for which $P_P(X_J, Y_J)$ depends only on the position of the journal center and can be calculated using the direct solution of Reynolds Eq. (2) when $\frac{\partial H}{\partial\tau} = 0$. $P_{X'}$ and $P_{Y'}$ can be calculated by differentiation of Eq. (2) with respect to X_J' and Y_J' respectively, as follows

$$\frac{\partial}{\partial\phi}\left(H^3\frac{\partial P_{X'}}{\partial\phi}\right)+\frac{\partial}{\partial Z}\left(H^3\frac{\partial P_{X'}}{\partial Z}\right) = 2\sin\phi, \tag{6}$$

$$\frac{\partial}{\partial\phi}\left(H^3\frac{\partial P_{Y'}}{\partial\phi}\right)+\frac{\partial}{\partial Z}\left(H^3\frac{\partial P_{Y'}}{\partial Z}\right) = 2\cos\phi. \tag{7}$$

The pressure gradients $P_{X'}, P_{Y'}$ can be evaluated through integration of Eqs. (6)–(7). To solve Eqs. (2), (6)–(7), the bearing surface is discretized as shown in Fig. 1-b, then integrated using finite difference method. By evaluation of $P_P, P_{X'}, P_{Y'}$, the bearing forces can be evaluated using the relation

$$\begin{aligned}F_X &= \int_0^{\frac{L}{R}}\int_0^{2\pi} -P\sin\phi\,\mathrm{d}\phi\,\mathrm{d}Z\\ &= \int_0^{\frac{L}{R}}\int_0^{2\pi} -\left(P_P+P_{X'}X_J'+P_{Y'}\,Y_J'\right)\sin\phi\,\mathrm{d}\phi\,\mathrm{d}Z = F_{X_P}+C_{XX}X_J'+C_{XY}Y_J',\end{aligned} \tag{8}$$

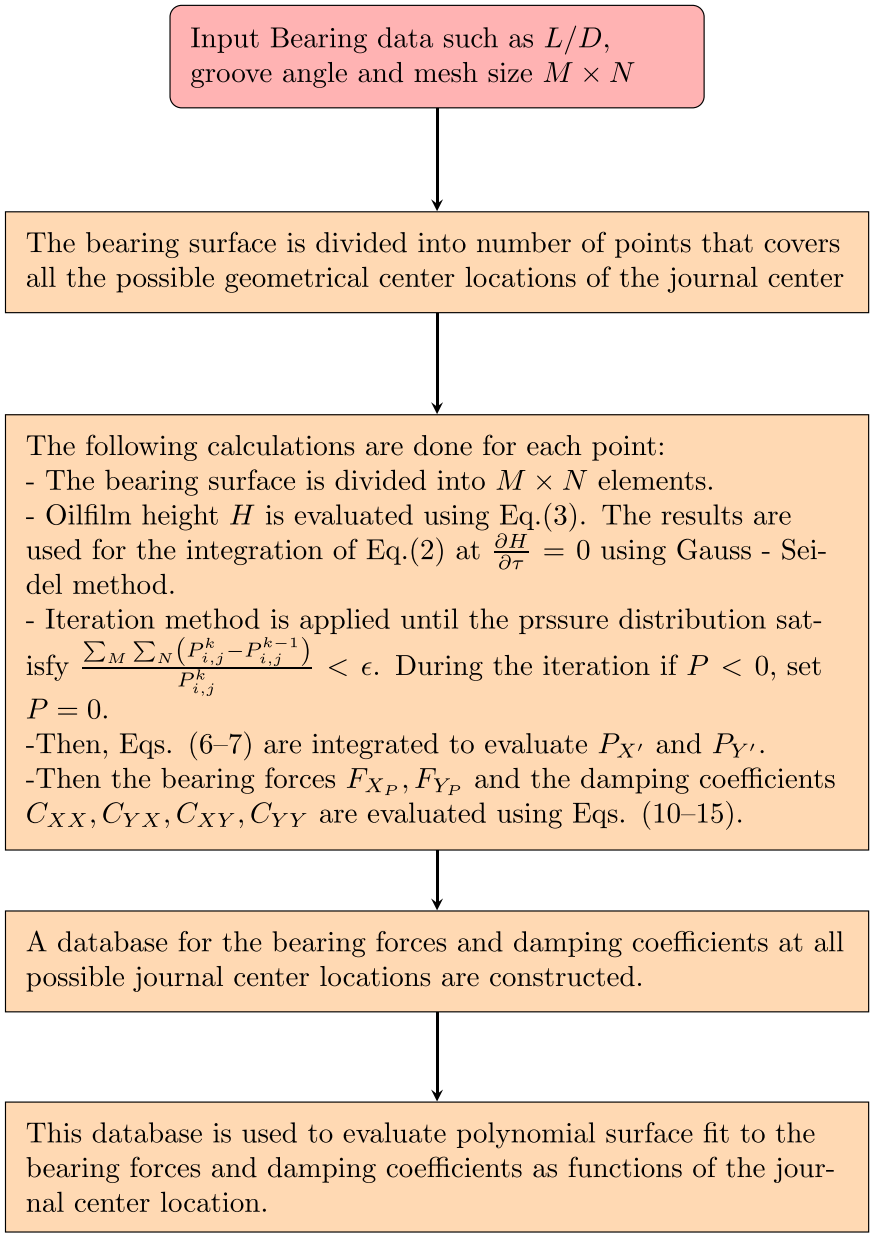

Fig. 2. Flow chart for present PFFLB analysis.

$$F_Y = \int_0^{\frac{L}{R}} \int_0^{2\pi} -P\cos\phi \, \mathrm{d}\phi \, \mathrm{d}Z$$
$$= \int_0^{\frac{L}{R}} \int_0^{2\pi} -\left(P_P + P_{X'} X_J^{'} + P_{Y'} \, Y_J^{'}\right)\cos\phi \, \mathrm{d}\phi \, \mathrm{d}Z = F_{Y_P} + C_{YX} X_J^{'} + C_{YY} Y_J^{'}. \tag{9}$$

Using Eqs. (8)–(9), we can find the following coefficients

$$F_{X_P} = \int_0^{\frac{L}{R}} \int_0^{2\pi} -P_P \sin\phi \quad \mathrm{d}\phi \quad \mathrm{d}Z, \tag{10}$$

$$F_{Y_P} = \int_0^{\frac{L}{R}} \int_0^{2\pi} -P_P \cos\phi \quad \mathrm{d}\phi \quad \mathrm{d}Z, \tag{11}$$

$$C_{XX} = \int_0^{\frac{L}{R}} \int_0^{2\pi} -P_{X'} \sin\phi \quad \mathrm{d}\phi \quad \mathrm{d}Z, \tag{12}$$

$$C_{YX} = \int_0^{\frac{L}{R}} \int_0^{2\pi} -P_{X'} \cos\phi \quad \mathrm{d}\phi \quad \mathrm{d}Z, \tag{13}$$

$$C_{XY} = \int_0^{\frac{L}{R}} \int_0^{2\pi} -P_{Y'} \sin\phi \quad \mathrm{d}\phi \quad \mathrm{d}Z, \tag{14}$$

$$C_{YY} = \int_0^{\frac{L}{R}} \int_0^{2\pi} -P_{Y'} \cos\phi \quad \mathrm{d}\phi \quad \mathrm{d}Z. \tag{15}$$

In this approach, the journal bearing surface is divided into number of points that covers all the possible rotor geometrical center locations X_J and Y_J. The bearing forces F_{X_P}, F_{Y_P} and the damping coefficients C_{XX}, C_{YX}, C_{XY}, C_{YY} are evaluated at these points. Then, polynomial surface fitting is used to evaluate the bearing forces as a function of X_J and Y_J positions. The surface function F_{X_P} can be simply used to evaluate the journal equilibrium position at any load or eccentricity ratio accurately. Considering the fact that $x_1 = \varepsilon\sin(\theta)$ and $x_3 = \varepsilon\cos(\theta)$, the equilibrium position can be evaluated by equating $F_{X_P}(x_1, x_3) = 0$. Then, at any

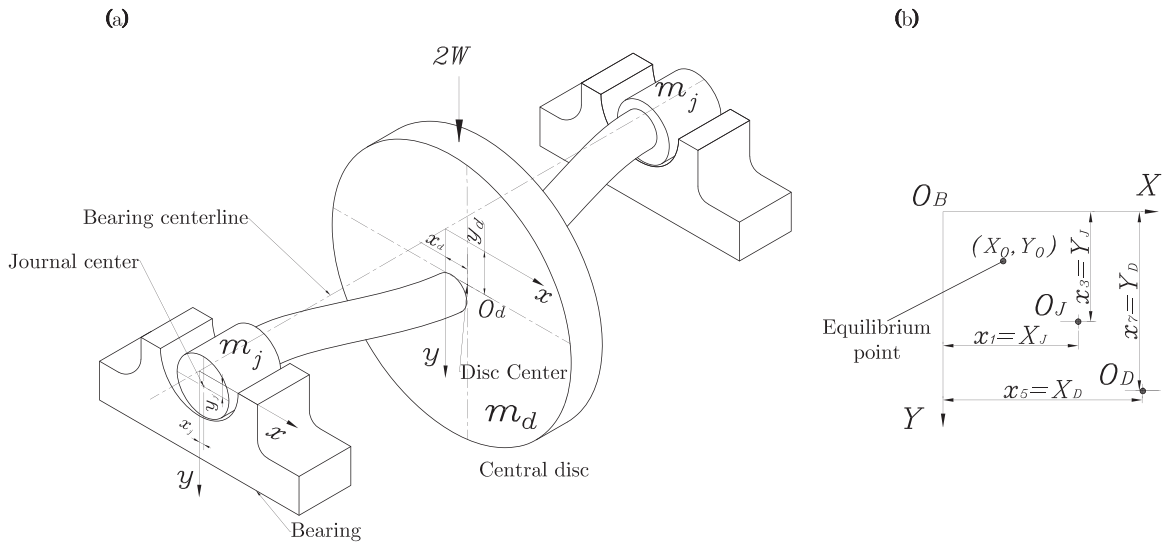

Fig. 3. (a) Elastic rotor supported on two symmetric journal bearings. (b) Dimensionless bearing coordinates.

eccentricity ratio the attitude angle which validate $F_{X_p} = 0$ can be obtained using Newton-Raphson technique. Moreover,the corresponding F_{Y_p} is the bearing load. Through the rest of the paper, this proposed method will be called polynomial fit-finite length bearing (PFFLB). A flow chart for the steps adopted in the PFFLB analysis is presented in Fig. 2.

2.2. Dynamical model

Here, the elastic rotor bearing model shown in Fig. 3 is selected to present the applicability of the proposed PFFLB journal bearing model. This elastic rotor bearing model consists of two equal journal masses m_j and single disc mass m_d. These masses are allowed to move in x and y directions. Therefore, the model can be approximated as four-degree of freedom model. The disc is located in the middle of the rotor, therefore the disc gyroscopic effect can be ignored.

The equations of motion for the elastic rotor bearing system can be described as follows:

$$\begin{aligned} &2m_j\ddot{x}_j + k_s\left(x_j - x_d\right) = -2F_x,\\ &2m_j\ddot{y}_j + k_s\left(y_j - y_d\right) = -2F_y,\\ &m_d\ddot{x}_d + k_s\left(x_d - x_j\right) = 0,\\ &m_d\ddot{y}_d + k_s\left(y_d - y_j\right) = 2W, \end{aligned} \tag{16}$$

where F_x and F_y are the forces resulted from the oil film pressure in x and y directions respectively. The rotating shaft lateral stiffness is k_s and the applied static load is $2W$. The geometrical center for the journal mass is x_j, y_j and the geometrical center for the rotating disc is x_d, y_d and these positions are evaluated with respect to the journal bearing geometric center O_b in Fig. 3-a. The total mass of the disc and the shaft is $m = m_d + 2m_j$. Eq. (16) can be transformed to the dimensionless form as follows:

$$\begin{aligned} &2M_J X_J'' + K_S(X_J - X_D) = -2\overline{F}_X,\\ &2M_J Y_J'' + K_S(Y_J - Y_D) = -2\overline{F}_Y,\\ &M_D X_D'' + K_S(X_D - X_J) = 0,\\ &M_D Y_D'' + K_S(Y_D - Y_J) = 2, \end{aligned} \tag{17}$$

where X_J

$$= \frac{x_j}{c},\ Y_J = \frac{y_j}{c},\ X_D = \frac{x_d}{c},\ Y_D = \frac{y_d}{c},\quad ' = \frac{d}{d\tau},\quad '' = \frac{d^2}{d\tau^2}, \tau = \Omega t,$$

$X_J'' = \frac{\ddot{x}_j}{\Omega^2 c}$, $Y_J'' = \frac{\ddot{y}_j}{\Omega^2 c}$, $X_D'' = \frac{\ddot{x}_d}{\Omega^2 c}$, $Y_D'' = \frac{\ddot{y}_d}{\Omega^2 c}$, $\overline{F}_X = \frac{F_x}{W} = \frac{F_X}{\overline{W}}$, $\overline{F}_Y = \frac{F_y}{W} = \frac{F_Y}{\overline{W}}$, $K_S = \frac{k_s}{W}\frac{c}{}$, $M_J = \frac{m_j\Omega^2 c}{W}$, $M_D = \frac{m_d\Omega^2 c}{W}$, for which $\overline{W} = \frac{L/D}{3\pi S}$ is the dimensionless load for finite bearing, $S = \frac{\mu\Omega r L}{\pi W}\left(\frac{r}{c}\right)^2$ is the Sommerfeld number.

The following mass ratios are considered in the current paper $M_J = 0.05\overline{M}$ and $M_D = 0.9\overline{M}$ for which $\overline{M} = \frac{m}{W}\frac{\Omega^2 c}{}$ is the total dimensionless mass of the rotor. Then, Eq. (17) can be written in the state space form as follows

$$\begin{aligned} x_1' &= x_2,\\ x_2' &= \frac{K_s(x_5 - x_1)}{2M_J} - \frac{\overline{F}_X}{M_J},\\ x_3' &= x_4,\\ x_4' &= \frac{K_s(x_7 - x_3)}{2M_J} - \frac{\overline{F}_Y}{M_J},\\ x_5' &= x_6,\\ x_6' &= \frac{K_s(x_1 - x_5)}{M_D},\\ x_7' &= x_8,\\ x_8' &= \frac{2 + K_s(x_3 - x_7)}{M_D}, \end{aligned} \tag{18}$$

where x_1

$= X_J$, $x_2 = X_J'$, $x_3 = Y_J$, $x_4 = Y_J'$, $x_5 = X_D$, $x_6 = X_D'$, $x_7 = Y_D$, $x_8 = Y_D'$.

.

Eq. (18) can be written as

$$\mathbf{x}' = \mathbf{f}(\mathbf{x},\quad \overline{M}), \tag{19}$$

where $\mathbf{x} = [x_1\ \ x_2\ \ x_3\ \ x_4\ \ x_5\ \ x_6\ \ x_7\ \ x_8]$. Fourth/fifth Runge-Kutta direct numerical integration method is used to solve the coupled differential equations and to evaluate the response of the dynamical system Eq. (18).

3. Results and discussions

The results Section is divided into four main subsections. In the first subsection, the bearing mesh sensitivity and the number of points used to evaluate the force and damping coefficients are investigated. In the second subsection, the bearing forces and damping coefficients surface fit results are presented. Then, a perturbation analysis is presented to investigate the accuracy of the present model in evaluating the bearing nonlinear forces against that evaluated using direct solution of Reynolds

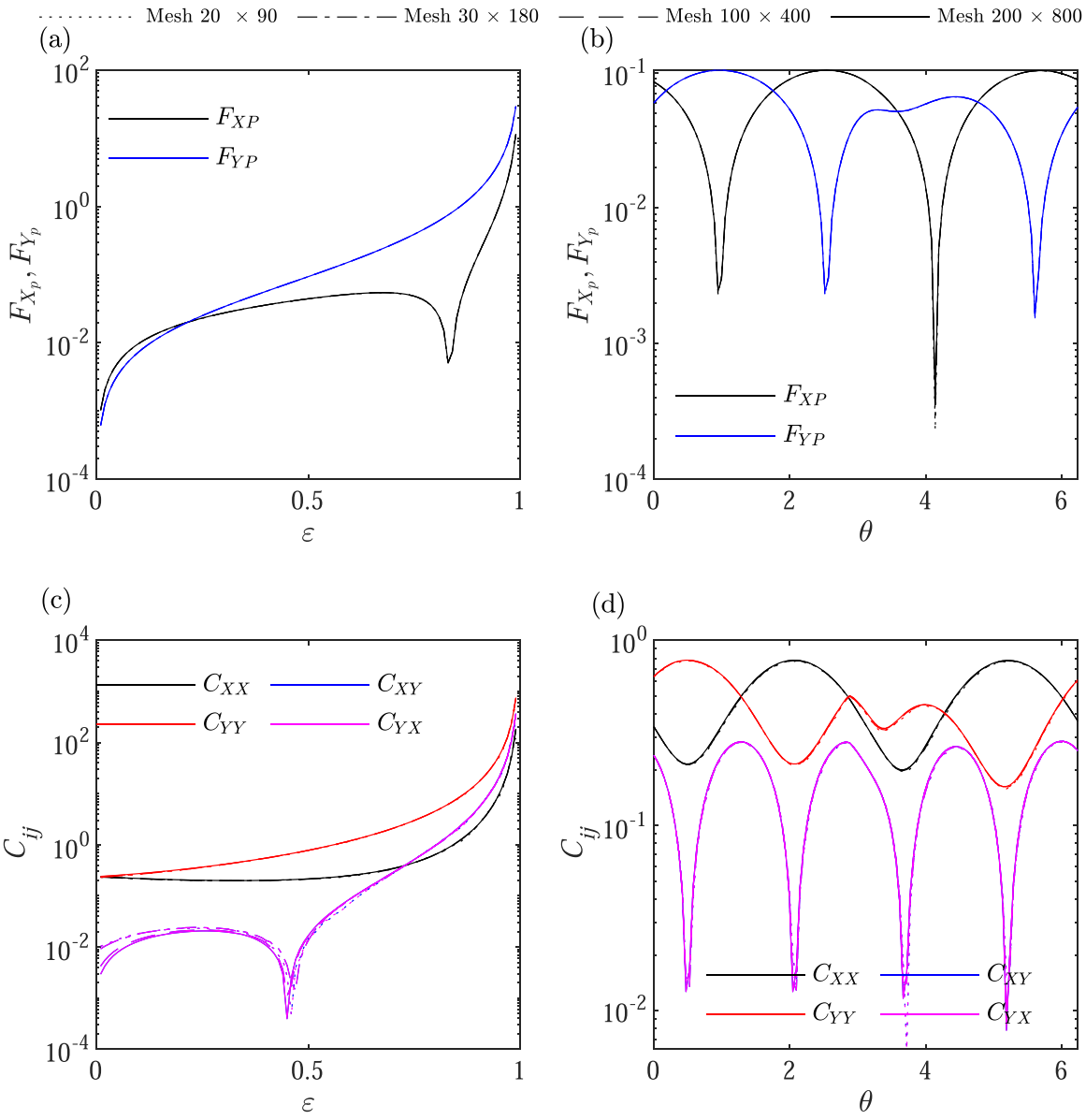

Fig. 4. Semi-log plot for the dimensionless force components F_{X_p} and F_{Y_p} (a, b) and bearing coefficients (c, d) versus eccentricity ratio (a, c) and attitude angle (b, d). The Figure is prepared using four mesh sizes as (20 × 90, 30 × 180, 100 × 400 and 200 × 800).

equation. In the last section, the present bearing model is used to analyze the dynamics of rotor supported in two symmetric journal bearings which is presented in the Section 2.2. Rotor- bearing stability analysis, numerical continuation and time response results are discussed. The bearing model adopted in the results section is based on $L/D = 0.5$ to allow the comparison of the results with short bearing results. However, the present analysis is not limited to specific L/D ratio.

3.1. Effect of mesh size and data-points on the evaluated forces

In this section, the effect of the mesh size used for solving the Reynolds equation on the evaluated force and damping coefficients are investigated. Also, the number of selected points, in the bearing domain, used to evaluate the fitting polynomial function is investigated.

3.1.1. Effect of mesh size

The mesh size used to solve the Reynolds equation is one of the important parameters. Very fine mesh results in computationally expensive solution and coarse mesh results in inaccurate solution. Therefore the effect of mesh size on the evaluated forces and damping coefficients are investigated. Four mesh sizes ranges from coarse to fine are selected as (20 × 90, 30 × 180, 100 × 400 and 200 × 800). The force components and the bearing coefficients are evaluated using these mesh sizes at two lines in the bearing physical domain ($\varepsilon \in 0$–1, $\theta \in 0$–2π). The first line is selected at constant attitude angle of ($\theta = \pi/6$) and variable eccentricity ratio($\varepsilon \in 0$–1). This is plotted in Fig. 4 (a, c) in the left column. The second line is evaluated at constant eccentricity ratio ($\varepsilon = 0.5$) and an attitude angle ($\theta \in 0$–2π). This is plotted in Fig. 4 (b, d) in the right column. From the results of Fig. 4, it can be concluded that both mesh sizes of 100 × 400 and 200 × 800 results are approximately coincident. Therefore, a mesh size of 100 × 400 are considered during the present work.

3.1.2. Effect of size of data points

In the present analysis the physical journal bearing domain is discretized into several points in both eccentricity ratio ε and attitude angle θ. At these points, the force and damping coefficients are evaluated using Eqs. (10)–(15). The effect of changing the number of points used to

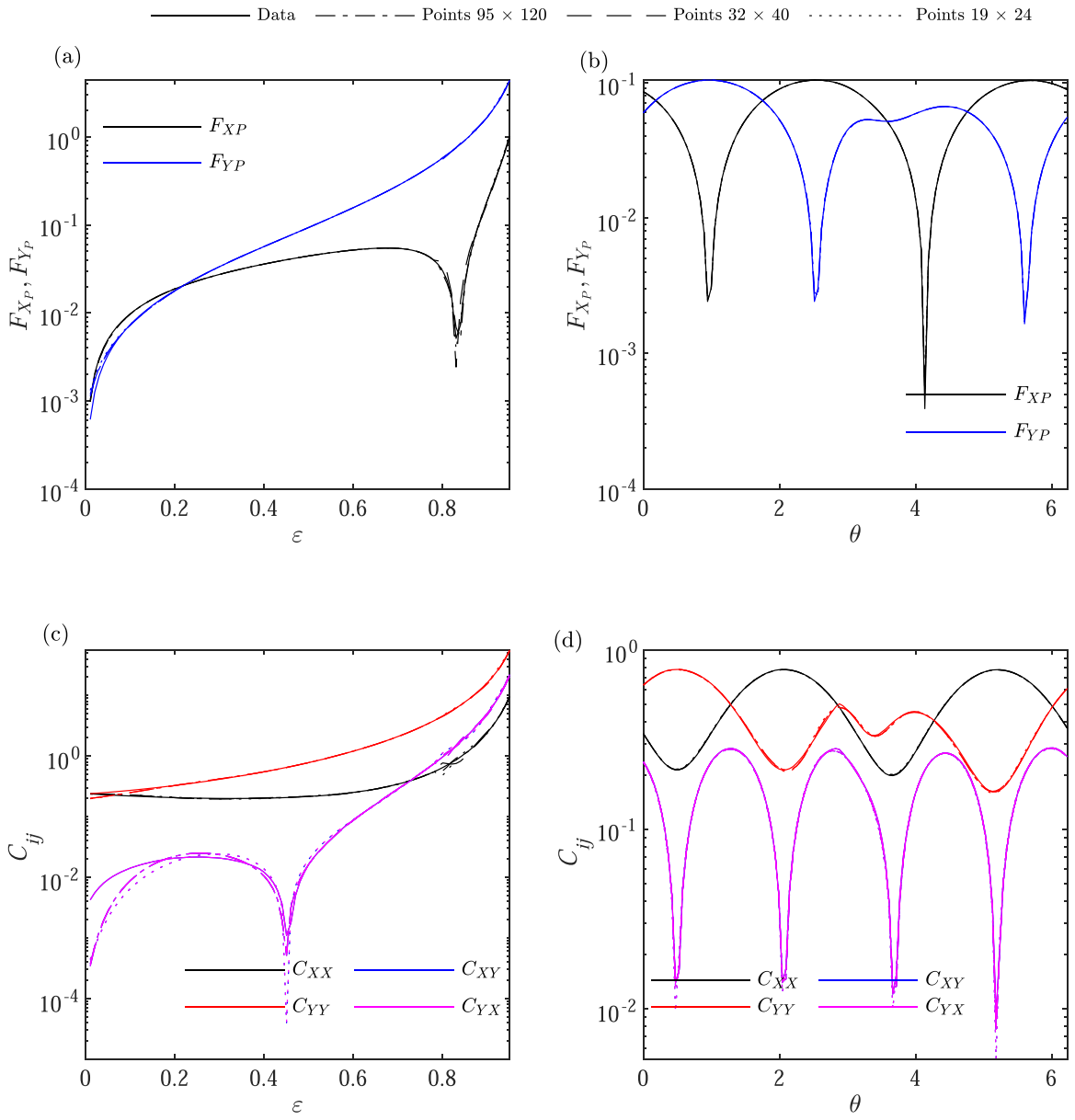

Fig. 5. Semi-log plot for the dimensionless force components F_{X_P} and F_{Y_P} (a, b) and bearing coefficients (c, d) versus eccentricity ratio (a, c) and attitude angle (b, d). The Figure is prepared using the evaluated data (solid line) and the polynomial surface fit based on 95 × 120 points, 32 × 40 points and 19 × 24 points.

create this dataset is investigated. This is done by using three datasets of size (19 × 24, 32 × 40 and 95 × 120). The computational time for evaluating these datasets are 1615, 4480 and 40,353 s respectively. These datasets are then processed to obtain the polynomial surface fitting for the force components and damping coefficients as will be shown in the following section. Here, fitting equations are evaluated based on different size of these datasets. The results of these obtained fitting equations are evaluated along with the original data-points in the domain ($\varepsilon \in [0–0.95]$ and $\theta \in [0–2\pi]$). Two line cases are selected, the first line case is at constant attitude angle of ($\theta = \pi/6$) and $\varepsilon \in [0–0.95]$ Fig. 5 left column and the second line case is at constant eccentricity ratio $\varepsilon = 0.5$ and $\theta \in [0–2\pi]$ Fig. 5 right column. Fig. 5 show that using datasets of 95 × 120 results in very close proximity between polynomial fitting and the original data results. It is worth noting that the fitting surface for each parameter is done in two steps, the first step is $\varepsilon \in [0–0.8]$ and the second step is $\varepsilon \in [0.8–0.95]$. This is because the gradient of force is very steep in the boundaries of the clearance circle which make it difficult to reach a single polynomial to accurately fit the whole domain.

3.2. Polynomial fit of bearing forces

From the analytical section Eqs. (8)–(9), it can be found that the total bearing forces are functions in the state variables $X_J, Y_J, X_J^{'}, Y_J^{'}$ which represent the journal center position and velocity, respectively. In addition, the bearing forces depend on the bearing parameters such as the slenderness ratio L/D ratio and groove angle. In this section, the bearing forces F_{X_P}, F_{Y_P} and the bearing damping coefficients C_{XX}, C_{YX}, C_{XY}, C_{YY} are evaluated at all possible journal geometrical center locations. These coefficients are evaluated for the ungrooved circular bearing with $L/D = 0.5$ and they are presented in Fig. 6. The surface polynomial fit for the bearing forces F_{X_P}, F_{Y_P} and damping coefficients C_{XX}, C_{YX}, C_{XY}, C_{YY} as functions of journal position are evaluated for the present case. The eccentricity ratio ε is divided into 95 points and the circumference coordinate ϕ is divided into 120 points to perform 11,400 points as discussed in the previous section. Then the cartesian positions $X_J = \varepsilon\sin\phi$ and $Y_J = \varepsilon\cos\phi$ are evaluated at each point. After that the bearing forces F_{X_P}, F_{Y_P} and damping coefficients

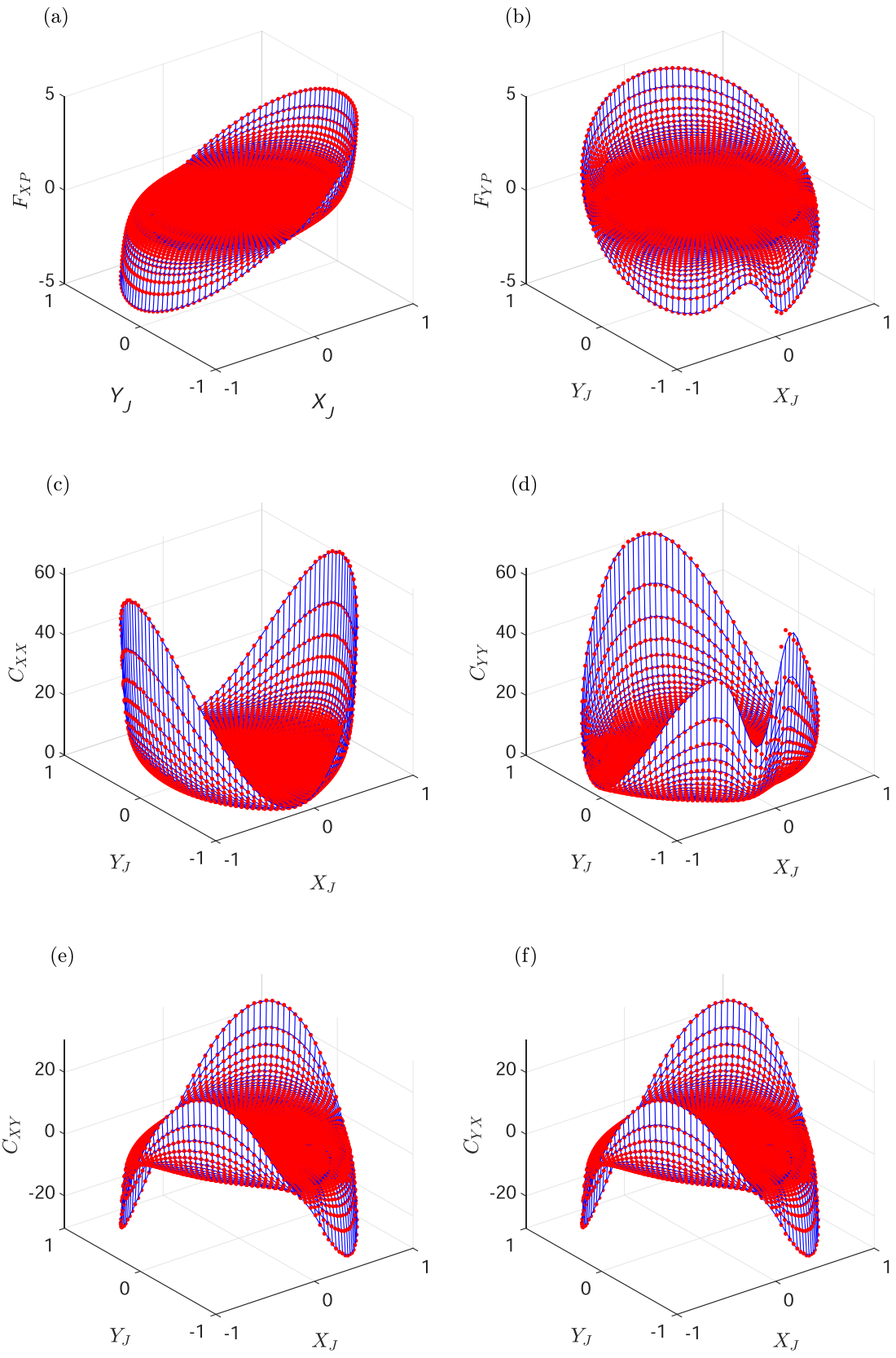

Fig. 6. Three dimensional plot for the bearing forces and damping coefficients data points and polynomial fitting surfaces (a) F_{X_P}, (b) F_{Y_P}, (c) C_{XX}, (d)C_{YY}, (e) C_{XY}, (f) C_{YX}. The fitting polynomial surface are evaluated as functions of journal position X_J, Y_J, for ungrooved circular bearing with $\frac{L}{D} = 0.5$.

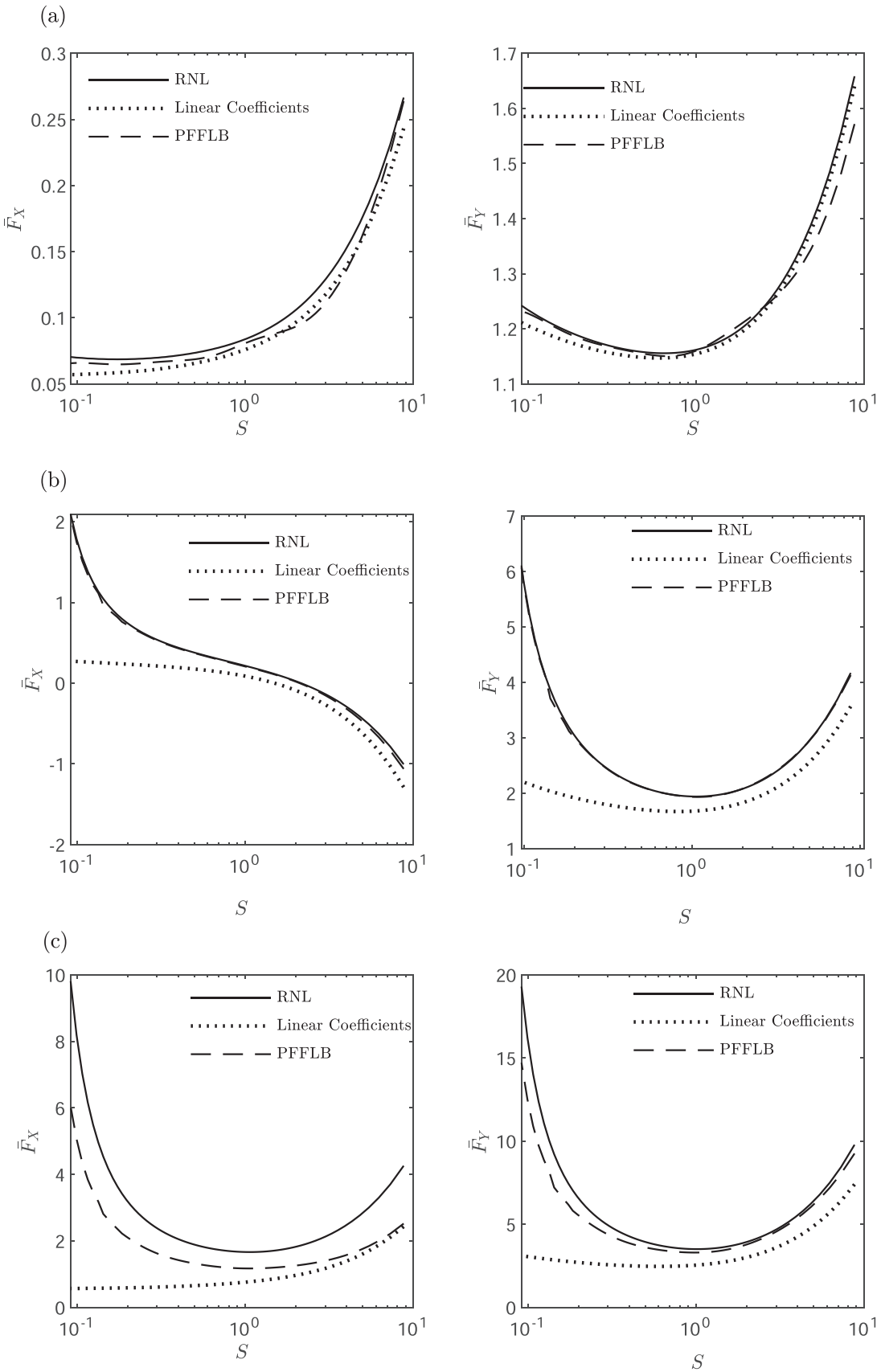

Fig. 7. Semi-log plot for the dimensionless force components $\overline{F}_X$ and $\overline{F}_Y$ versus Sommerfeld number. These forces are resulted from journal perturbation from the equilibrium position in X and Y directions for ungrooved journal bearing with $L/D = 0.5$ (a) $(\delta X = 0.01, \delta X' = 0.01, \delta Y = 0.01$ and $\delta Y' = 0.01)$, (b)$(\delta X = 0.1, \delta X' = 0.01, \delta Y = 0.1$ and $\delta Y' = 0.01)$ and (c) $(\delta X = 0.1, \delta X' = 0.1, \delta Y = 0.1$ and $\delta Y' = 0.1)$.

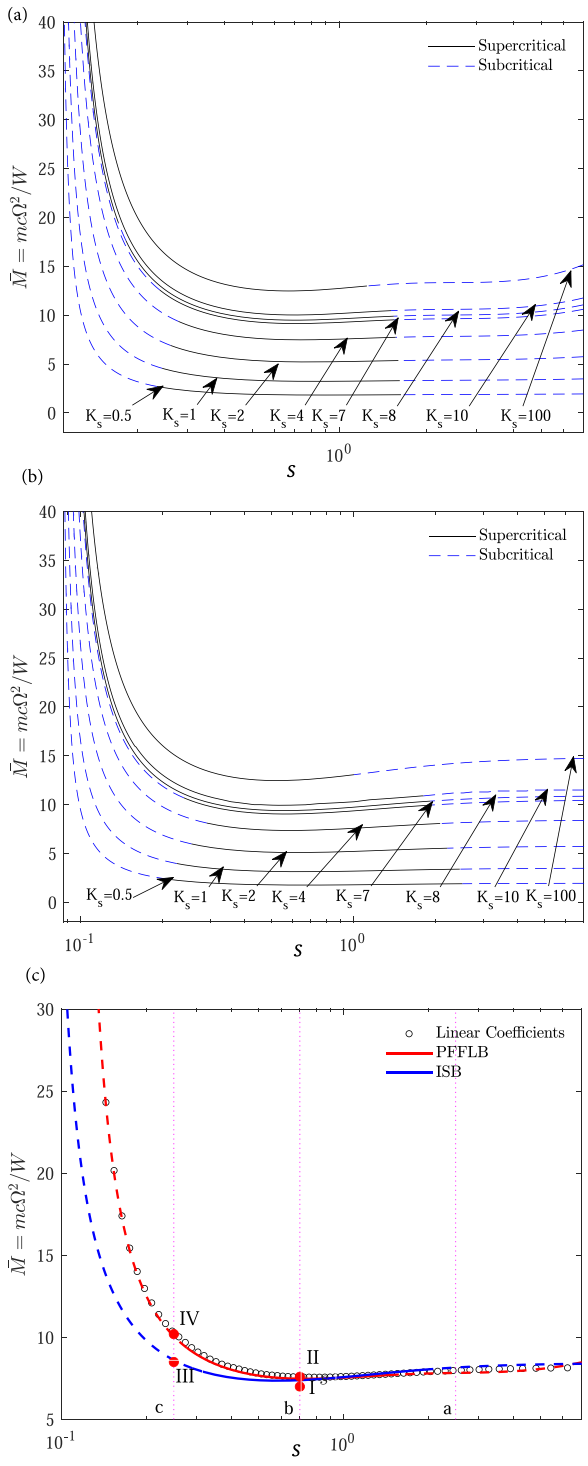

Fig. 8. Flexible rotor-bearing stability curves: (a) Threshold dimensionless-mass versus Sommerfeld No. analysis based on PFFLB at $L/D = 0.5$. (b) Threshold dimensionless mass versus Sommerfeld No. based on ISB. (c) Threshold mass versus Sommerfeld No. for $K_S = 4$ based on PFFLB, ISB and bearing linear coefficients.

C_{XX}, C_{YX}, C_{XY}, C_{YY} are calculated at these 11,400 points. Then surface polynomial fits are used for these parameters as functions of the journal position. In addition, the surface fittings for these points and for each parameter are plotted in the same figure as shown in Fig. 6(a–f). The results of Fig. 6 show that both the surface fitting and data points are matched very well. The six polynomial surface equations for the two force components and the four damping parameters when $\varepsilon \in [0–0.8]$ are listed in Appendix A.

3.3. Force perturbation

In this section, a perturbation analysis is done to investigate the accuracy of the proposed analysis in evaluating the nonlinear bearing forces. The results are evaluated based on three methods which are direct solution of Reynolds equation (RNL), linear bearing coefficients and the present PFFLB method. The results are evaluated for three perturbation cases from the equilibrium position as shown in Fig. 7 which are (a) ($\delta X = 0.01, \delta X' = 0.01, \delta Y = 0.01$ and $\delta Y' = 0.01$), (b) ($\delta X = 0.1, \delta X' = 0.01, \delta Y = 0.1$ and $\delta Y' = 0.01$) and (c) ($\delta X = 0.1$, $\delta X' = 0.1, \delta Y = 0.1$ and $\delta Y' = 0.1$). The figure results show that at low perturbations the forces evaluated using all the four methods are approximately the same as shown in Fig. 7 (a). The figure results show that for the investigated cases the PFFLB results are closer to RNL results compared with linear bearing coefficients method. In case (b) smaller velocity perturbation is used compared with that used in case (c). Comparing case(b) and case (c) results, the reader can realize that the deviation of the present PFFLB from RNL increases in case (c). However, the final evaluated forces are better than that based on traditional linear bearing coefficients.

3.4. Dynamical results

3.4.1. Stability analysis

In this section, the stability analysis of the elastic Jeffcott rotor-bearing system, which is shown in Fig. 3, is investigated. At the beginning, the Hopf bifurcation of the autonomous dynamical system, which is presented in Eq. (18), is studied using the proposed PFFLB approximation of bearing forces for ungrooved bearing with $L/D = 0.5$. The same case is solved based on infinitely short bearing (ISB) approximation, see for example [8,44]. Both solutions are compared together.

From Eq. (18), it can be realized that the parameters which influence the present dynamical system are the dimensionless mass $\overline{M}$, the dimensionless stiffness K_s and Sommerfeld number S. Therefore, the dynamical system Eq. (19) can be written as $\dot{\mathbf{x}} = f(\mathbf{x}, \quad \overline{M}, S, K_s)$.

The Hopf bifurcation of the dynamical system which is modeled by Eq. (18), is investigated using numerical continuation. When Hopf bifurcation occurs, limit cycle starts to be formed and numerical continuation can also be used for the identification of whether these limit cycles are stable or not. Here, continuation analysis is performed using MATCONT toolbox which is written using MATLAB software [45]. Initially, the equilibrium position is identified at conditions below the threshold speed for a specific condition with constant Sommerfeld number S and dimensionless stiffness K_s. Then, one variable $\overline{M}$ continuation is performed to evaluate the Hopf bifurcation point. After that, the Hopf bifurcation line is identified using two parameters $(\overline{M}, S)$ continuation analysis and at constant K_s. The type of Hopf bifurcation whether supercritical or subcritical can be identified using the MATCONT toolbox based on the first coefficient of Lyapunov exponent. When the first coefficient of Lyapunov has positive sign, the bifurcation type is subcritical Hopf bifurcation and when the first coefficient of Lyapunov has negative sign, the bifurcation type becomes supercritical Hopf bifurcation. Fig. 8 a, b show the results of Hopf bifurcation analysis for flexible rotor model using PFFLB and ISB methods respectively. The vertical axis of the figure represents the threshold mass $\overline{M}$ and the horizontal axis represents the Sommerfeld number. The stability results are evaluated using several values of dimensionless shaft stiffness coefficients ranges from $K_s \in [0.5–100]$ which covers the range between flexible to rigid rotor. As presented in Fig. 8 a and b, there is a good agreement between the stability results that obtained based on the polynomial approximation and that obtained based on short bearing approximation at $L/D = 0.5$. Fig. 8-c presents the results of selected case of $K_S = 4$. For this case, the stability curve for the dynamical system is

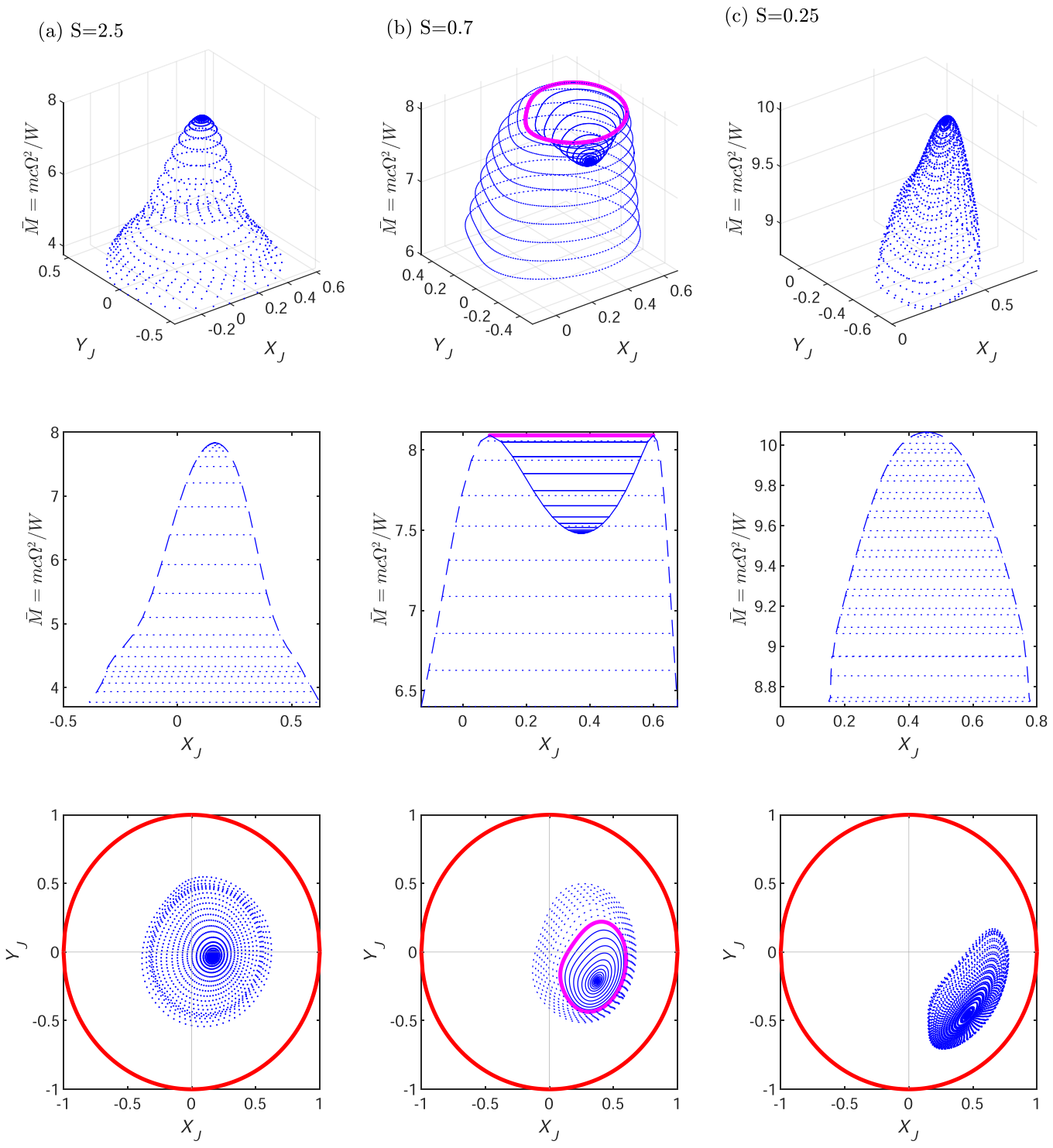

Fig. 9. Continuation results of the dynamic model using present PFFLB force approximation, $K_s = 4$, $L/D = 0.5$, using different Sommerfeld numbers (a) $S = 2.5$ (first column), (b) $S = 0.7$ (second column), (c) $S = 0.25$ (third column). The 3D presentation of limit cycles is shown first row, section plot of the limit cycles is displayed in the second row and the top view of the limit cycles is displayed in the third row.

evaluated using three methods. In these methods the bearing forces are evaluated using PFFLB, ISB and first order bearing coefficients [29]. The results show that the values of the threshold speed evaluated based on present PFFLB are very close to that evaluated based bearing coefficients and there is minor deviations from that evaluated based on ISB approximation.

3.4.2. *Continuation results*

In this section, the dynamics of the flexible rotor supported on two symmetric journal bearings are investigated using numerical continuation. The dynamical model equations of motion in Eq. (18) are used for the continuation analysis. The PFFLB and ISB approximations for bearing forces are used for the continuation analysis. Continuation analysis is performed using the MATCONT toolbox [45] in MATLAB language.

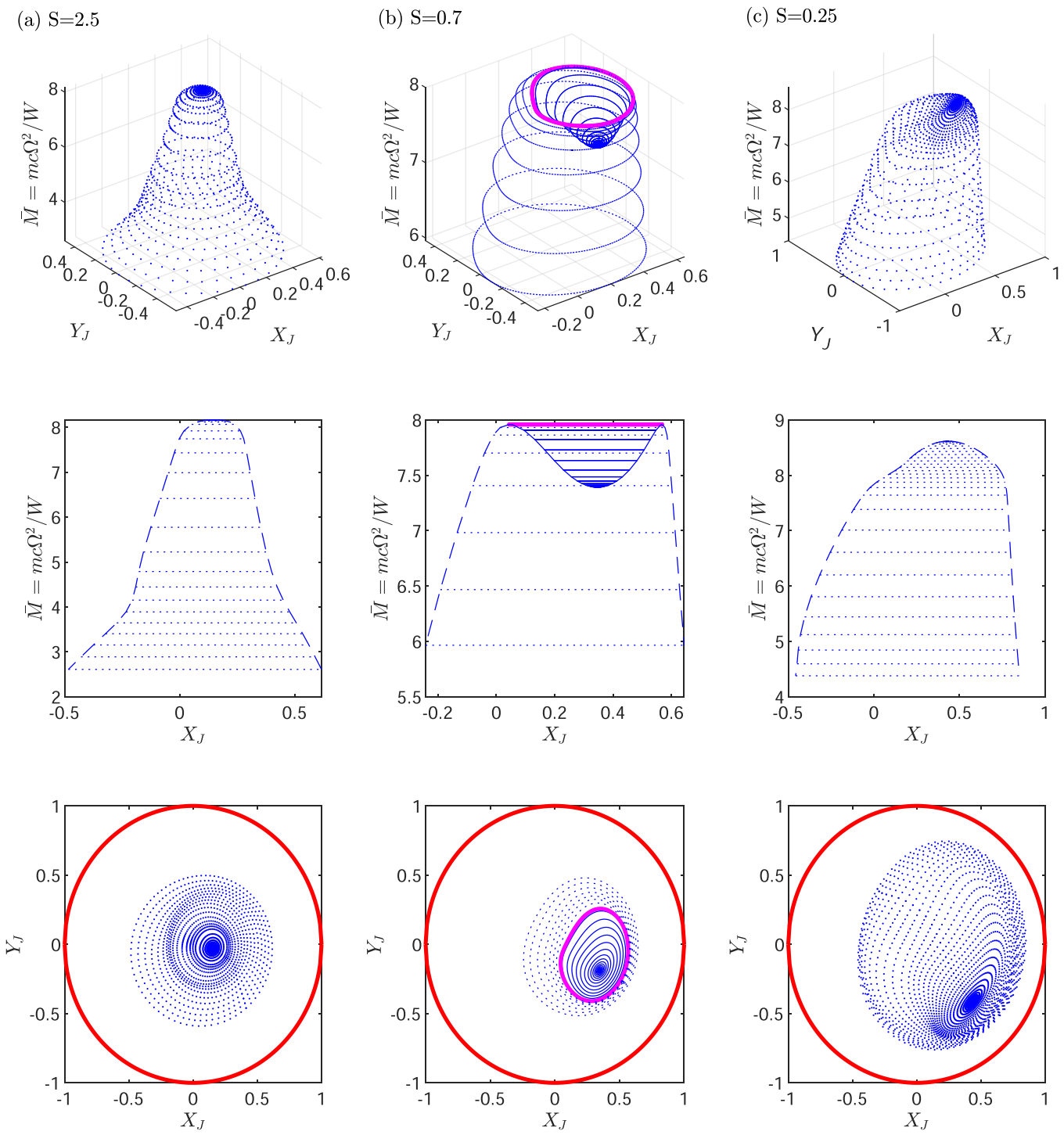

Fig. 10. Continuation results of the dynamic model using ISB approximation, $K_s = 4$, and using different Sommerfeld numbers (a) $S = 2.5$ (first column), (b) $S = 0.7$ (second column), (c) $S = 0.25$ (third column). The 3D presentation of limit cycles is shown first row, section plot of the limit cycles is displayed in the second row and the top view of the limit cycles is displayed in the third row.

Using the continuation analysis, the equilibrium point is initially identified numerically at a point below the threshold speed with constant Sommerfeld number S and dimensionless stiffness K_s. Then, the threshold mass is identified by applying one variable $\overline{M}$ continuation analysis where the threshold mass represents the commence of Hopf bifurcation. From the Hopf bifurcation point, the rotor dynamics are investigated using the limit cycle continuation analysis. Fig. 9 and Fig. 10 represent the limit cycle continuation analysis for $K_s = 4$ and Sommerfeld numbers $S = 2.5$, 0.7 and 0.25 (different static loads). In Fig. 9, the continuation analysis is based on PFFLB force approximation. Fig. 10 displays the results using ISB approximation. The results of both figures show that the continuation results of the limit cycles based on both PFFLB and ISB force approximation are similar.

The continuation analysis is applied at three different values of Sommerfeld number and at constant rotor stiffness as shown in Fig. 9 and Fig. 10 respectively. In Both Figs. 9, 10, the first column and the third column represent subcritical bifurcations at S = 2.5 (Case a), $S = 0.25$ (case c) respectively. This can be identified by the unstable

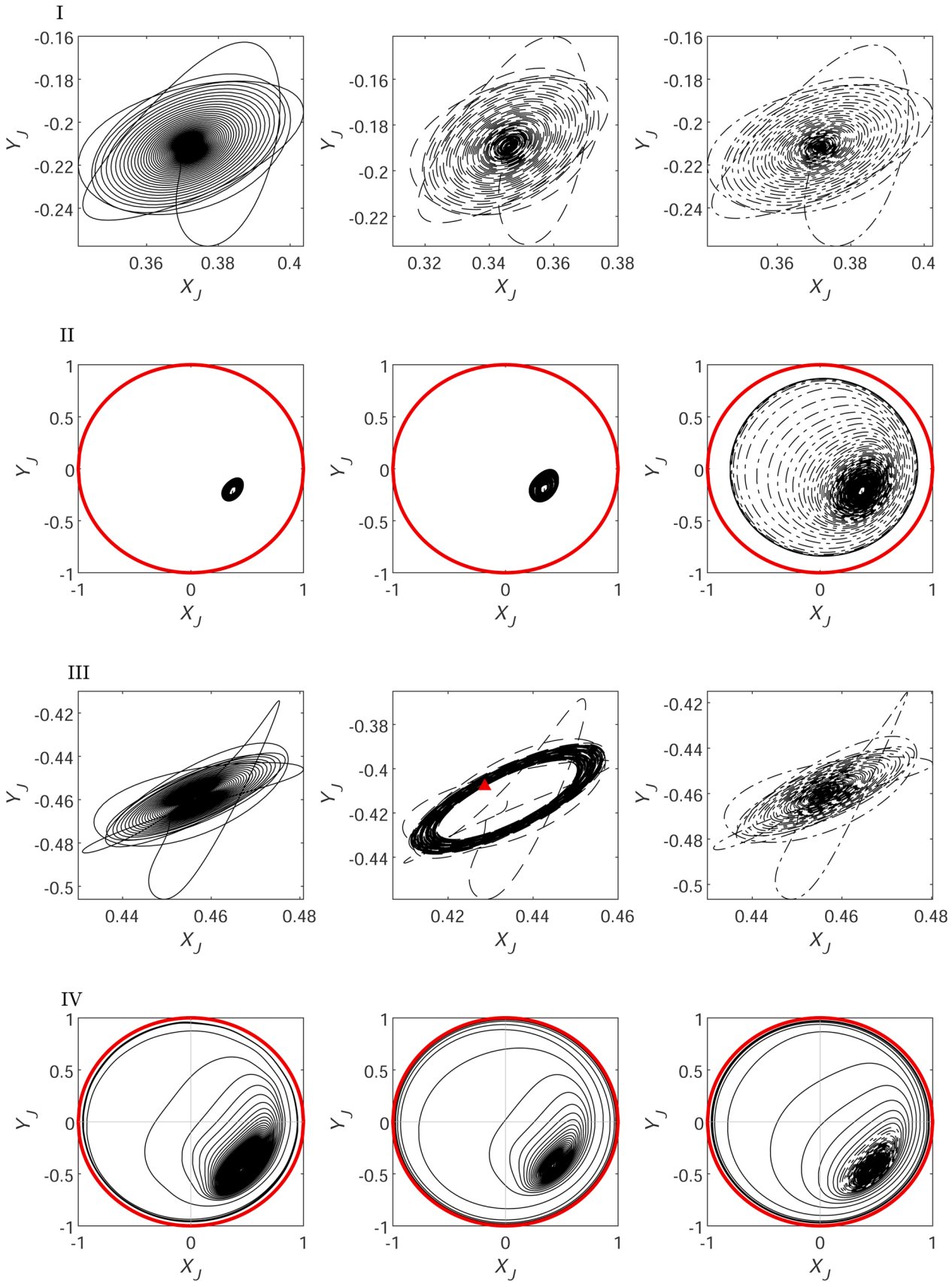

Fig. 11. Orbit plots of the journal center at different operating points, I, II, III and IV. For all cases PFFLP is shown in the first column, ISB is shown in the second and RNL is shown in the last column, $Ks = 4$; Init = [X_{J0} 0 Y_{J0} 0.1 X_{D0} 0 Y_{D0} 0.1] for which X_{J0}, Y_{J0}, X_{D0}, Y_{D0} are the equilibrium positions for the journal and central disc respectively.

Table 1
Computational time for numerical integration and evaluation of the time response results.

Case	S	$\overline{M}$	τ	Calculation time (s)		
				PFFLP	ISB	RNL
I	0.7	7	1000	1.248	0.786	431.77
II	0.7	7.6	3000	10.133	2.617	3444.32
III	0.25	8.5	1000	1.98	0.712	367.2
IV	0.25	10.2	5700	27.164	77.917	6913.64

limit cycles growth with the decrease of the non-dimensional mass $\overline{M}$.

However, for case b in the second column of Figs. 9, 10 a stable limit cycle is shown with the increase of the non-dimensional mass $\overline{M}$ above the Hopf bifurcation point at $\overline{M} = (7.48, 7.391)$ respectively. At $\overline{M} = (8.09, 7.959)$ in Figs. 9, 10 respectively, a limit cycle point is detected where the stable limit cycle converts to unstable limit cycle. It is worth noting that these limit cycles represent the basin of attraction for the journal center.

For unstable limit cycles if the initial condition is inside the basin of attraction, the solution will be attracted to the equilibrium point or limit cycle. Meanwhile, the solution will diverge if the initial condition is located out the basin of attraction. For stable limit cycles, the solution will be attracted to these limit cycles whether the initial condition is inside or outside the basin of attraction.

3.4.3. Time response results

In this section, selected orbit plots of the dynamical system shown in Eq. (18) are investigated. These orbit plots are displayed in Fig. 11. Three models of the bearing forces are used in this section. The first model is using PFFLP and shown in the first column. The ISB is the second model, and it is displayed in the middle column. The last model is the Reynolds nonlinear bearing model (RNL). Finite difference method with mesh 180×30 is used in the solution of this model. The RNL model results are presented in the last column. Four cases are selected to investigate the orbit plots of the journal center. These cases are shown in Fig. 8 (c) with points I, II, III and IV. All the cases are investigated at constant $L/D = 0.5$ and $K_s = 4$. Cases I and III are below the threshold speed and cases II and IV are above the threshold speed. Cases I and II are in the supercritical Hopf bifurcation region and cases III and IV are in the subcritical Hopf bifurcation region according to both PFFLP and ISB bearing models. The initial conditions for all response results are$[X_{J0}$ 0 Y_{J0} 0.1 X_{D0} 0 Y_{D0} 0.1] for which X_{J0}, Y_{J0}, X_{D0}, Y_{D0} are the equilibrium positions for the journal and central disc respectively.

The first row displays the results of case I for which $S = 0.7$ and $\overline{M} = 7$. As shown in Fig. 11, the three models of bearing forces give similar results for case I. Case II is displayed in the second row of Fig. 11 where $S = 0.7$ and $\overline{M} = 7.6$. Both PFFLP and ISB bearing force analyses give stable limit cycles as shown in the first two columns of the second row of Fig. 11. RNL analysis of case II gives initially similar limit cycle which then grows to a larger limit cycle.

Case III is introduced in the third row of Fig. 11 for which $S = 0.25$ and $\overline{M} = 8.5$. In case III, RNL and PFFLP give similar orbit plots where the journal center is stabilized in the equilibrium position. The orbit plot based on ISB for case III is stabilized in longer time where the threshold speed based on ISB is less than the threshold speed based on both PFFLP and RNL as shown in Fig. 8-c.

The last row of Fig. 11 displays the orbit plot of case IV where $S = 0.25$ and $\overline{M} = 10.2$. This case is subcritical Hopf bifurcation based on both PFFLP and ISB. The orbit plots of case IV show unstable limit cycles using the three models. Table 1 displays the calculation time for the four cases investigated. Runge-Kutta ODE45 MATLAB function is used in the solution of the dynamic system equations. As observed in Table 1, RNL requires larger computational time compared with PFFLP and ISB. ISB model shows the shortest computational time in cases I, II and III. For case IV, PFFLP model records smaller computational time compared with ISB. In case IV, the solution based on ISB is reached near the clearance circle before the solutions based on PFFLP and RNL because ISB has lower threshold speed at $S = 0.25$. Near the clearance circle the stiffness of the oil film becomes very high and this leads to longer computational time which explains why ISB requires longer time in case IV.

In general, the computational time for PFFLP method is relatively larger than that of ISB. However, PFFLP model has more advantage in that it can be used to model any bearing whether short, finite or long bearings. In addition, PFFLP method can be used for modeling the cases grooved and un-grooved bearing.

4. Conclusion

The present paper introduces a new analysis to evaluate the bearing non-linear forces. This analysis is introduced as start to solve the drawbacks of evaluating the bearing forces based on bearing coefficients where these coefficients are evaluated in the vicinity of the bearing static equilibrium position. In the bearing coefficient method, the solution accuracy is reduced above the threshold speed because limit cycles are started to form. Although the accuracy of coefficient method can be increased by increasing the order of coefficient but still a reasonable reduction in accuracy is monitored with increase of the size of the limit cycle and the journal center becomes far away from the equilibrium point.

In the present method, polynomial functions are evaluated to cover the bearing forces on all possible journal center locations. This enables more accurate evaluation of the bearing forces in any location. Furthermore, this analysis is possible for short, finite and long bearings. Moreover, the results of present polynomial fit-finite length bearing (PFFLP) method consume less computational time compared with RNL method while solving rotor-bearing dynamics as shown in Table 1. The limitation of the present model is that the polynomial fitting equations are suitable for a specific bearing geometry. Changing the bearing L/D ratio or adding internal grooves requires reevaluating of the polynomial function. However, for the same bearing geometry the polynomial equations are valid for different loading conditions. Moreover, The analysis can not be used for mixed and boundary lubrication conditions when the bearing supposed to contact with the journal clearance circle.

Declaration of Competing Interest

The authors declare that they have no known competing financial interests or personal relationships that could have appeared to influence the work reported in this paper.

Acknowledgements

None.

Appendix A. Polynomial fit equations

The fitting equation for the bearing forces F_{XP}, F_{YP} and four damping coefficients, C_{XX}, C_{YX}, C_{XY} and C_{YY} in terms of $x = X_J$, $y = Y_J$ are given by,

$$
\begin{aligned}
F_{X_P} = \; & 0.07624\,x^{12} + 4.508\,x^{11}\,y + 11.39\,x^{11} - 1.093\,x^{10}\,y^2 - 2.17\,x^{10}\,y - 0.1189\,x^{10} + 2.44\,x^9\,y^3 + 60.6\,x^9\,y^2 - 7.71\,x^9\,y \\
& -14.44\,x^9 - 0.3763\,x^8\,y^4 - 13.02\,x^8\,y^3 + 1.7\,x^8\,y^2 + 2.179\,x^8\,y + 0.06595\,x^8 + 3.735\,x^7\,y^5 + 117.0\,x^7\,y^4 - 2.871\,x^7\,y^3 \\
& -62.55\,x^7\,y^2 + 4.931\,x^7\,y + 8.579\,x^7 + 1.866\,x^6\,y^6 - 25.92\,x^6\,y^5 - 0.3252\,x^6\,y^4 + 11.34\,x^6\,y^3 - 0.8481\,x^6\,y^2 - 1.272\,x^6\,y \\
& -0.01277\,x^6 - 1.367\,x^5\,y^7 + 117.7\,x^5\,y^6 - 1.262\,x^5\,y^5 - 90.0\,x^5\,y^4 + 0.798\,x^5\,y^3 + 27.98\,x^5\,y^2 - 1.442\,x^5\,y - 2.019\,x^5 \\
& +3.041\,x^4\,y^8 - 26.21\,x^4\,y^7 - 2.234\,x^4\,y^6 + 16.5\,x^4\,y^5 + 0.6755\,x^4\,y^4 - 4.836\,x^4\,y^3 + 0.1704\,x^4\,y^2 + 0.08377\,x^4\,y \\
& +0.003298\,x^4 + 1.814\,x^3\,y^9 + 56.37\,x^3\,y^8 + 0.357\,x^3\,y^7 - 59.24\,x^3\,y^6 + 0.03698\,x^3\,y^5 + 26.51\,x^3\,y^4 + 0.103\,x^3\,y^3 \\
& -4.502\,x^3\,y^2 + 0.2089\,x^3\,y + 0.5728\,x^3 + 1.677\,x^2\,y^{10} - 13.19\,x^2\,y^9 - 1.708\,x^2\,y^8 + 10.9\,x^2\,y^7 + 0.8439\,x^2\,y^6 \\
& -4.566\,x^2\,y^5 - 0.1403\,x^2\,y^4 + 0.2623\,x^2\,y^3 + 0.01757\,x^2\,y^2 - 0.1863\,x^2\,y + 0.004552\,x^2 - 0.06636\,x\,y^{11} \\
& +11.47\,x\,y^{10} + 0.181\,x\,y^9 - 14.56\,x\,y^8 - 0.2714\,x\,y^7 + 8.75\,x\,y^6 + 0.1005\,x\,y^5 - 2.075\,x\,y^4 - 0.03111\,x\,y^3 + 0.6063\,x\,y^2 \\
& -0.007499\,x\,y + 0.009583\,x - 0.01959\,y^{12} - 2.364\,y^{11} - 0.004447\,y^{10} + 2.428\,y^9 + 0.008009\,y^8 - 1.329\,y^7 - 0.0102\,y^6 \\
& +0.08139\,y^5 - 0.0006003\,y^4 - 0.1667\,y^3 - 0.00164\,y^2 - 0.1192\,y + 3.103e - 7,
\end{aligned} \tag{A.1}
$$

$$
\begin{aligned}
F_{Y_P} = \; & -11.05\,x^{12} - 0.6737\,x^{11}\,y + 2.435\,x^{11} - 16.64\,x^{10}\,y^2 + 5.316\,x^{10}\,y + 21.96\,x^{10} + 6.387\,x^9\,y^3 + 10.61\,x^9\,y^2 + 0.5989\,x^9\,y \\
& -2.482\,x^9 - 26.65\,x^8\,y^4 + 54.95\,x^8\,y^3 + 24.32\,x^8\,y^2 - 4.709\,x^8\,y - 16.82\,x^8 - 4.763\,x^7\,y^5 + 27.43\,x^7\,y^4 - 5.768\,x^7\,y^3 \\
& -8.834\,x^7\,y^2 - 0.08673\,x^7\,y + 1.345\,x^7 - 16.9\,x^6\,y^6 + 111.0\,x^6\,y^5 + 29.86\,x^6\,y^4 - 55.83\,x^6\,y^3 - 12.24\,x^6\,y^2 + 2.835\,x^6\,y \\
& +6.257\,x^6 + 3.039\,x^5\,y^7 + 22.37\,x^5\,y^6 + 3.012\,x^5\,y^5 - 17.21\,x^5\,y^4 + 1.658\,x^5\,y^3 + 3.906\,x^5\,y^2 - 0.03161\,x^5\,y - 0.0801\,x^5 \\
& -13.05\,x^4\,y^8 + 116.8\,x^4\,y^7 + 17.04\,x^4\,y^6 - 86.48\,x^4\,y^5 - 11.51\,x^4\,y^4 + 25.57\,x^4\,y^3 + 2.43\,x^4\,y^2 - 0.4715\,x^4\,y - 1.184\,x^4 \\
& +4.952\,x^3\,y^9 + 8.553\,x^3\,y^8 - 2.669\,x^3\,y^7 - 8.348\,x^3\,y^6 - 0.03276\,x^3\,y^5 + 4.226\,x^3\,y^4 - 0.05424\,x^3\,y^3 - 0.2381\,x^3\,y^2 \\
& +0.02981\,x^3\,y + 0.1628\,x^3 + 7.901\,x^2\,y^{10} + 49.81\,x^2\,y^9 - 0.8073\,x^2\,y^8 - 54.93\,x^2\,y^7 - 1.562\,x^2\,y^6 + 24.59\,x^2\,y^5 \\
& +1.677\,x^2\,y^4 - 4.266\,x^2\,y^3 + 0.005071\,x^2\,y^2 + 0.3172\,x^2\,y + 0.1369\,x^2 + 7.568\,x\,y^{11} - 3.267\,x\,y^{10} - 7.186\,x\,y^9 \\
& +2.128\,x\,y^8 + 3.245\,x\,y^7 - 0.5304\,x\,y^6 - 0.2658\,x\,y^5 - 0.04752\,x\,y^4 + 0.1502\,x\,y^3 + 0.07727\,x\,y^2 + 0.05167\,x\,y + 0.09831\,x \\
& +0.9013\,y^{12} + 10.5\,y^{11} - 0.7346\,y^{10} - 13.54\,y^9 + 0.1165\,y^8 + 8.197\,y^7 + 0.1423\,y^6 - 1.996\,y^5 - 0.02657\,y^4 + 0.567\,y^3 \\
& +0.01282\,y^2 + 0.008132\,y + 0.0005587,
\end{aligned} \tag{A.2}
$$

$$
\begin{aligned}
C_{XX} = \; & 177.2\,x^{12} + 231.6\,x^{11}\,y - 4.85\,x^{11} + 872.5\,x^{10}\,y^2 + 1.796\,x^{10}\,y - 238.7\,x^{10} + 1222.0\,x^9\,y^3 - 26.34\,x^9\,y^2 \\
& -519.6\,x^9\,y + 9.187\,x^9 + 1634.0\,x^8\,y^4 + 13.1\,x^8\,y^3 - 911.3\,x^8\,y^2 - 3.647\,x^8\,y + 139.1\,x^8 + 2386.0\,x^7\,y^5 - 7.116\,x^7\,y^4 \\
& -2148.0\,x^7\,y^3 + 32.32\,x^7\,y^2 + 428.7\,x^7\,y - 6.448\,x^7 + 1579.0\,x^6\,y^6 - 5.404\,x^6\,y^5 - 1220.0\,x^6\,y^4 - 10.06\,x^6\,y^3 \\
& +378.6\,x^6\,y^2 + 2.45\,x^6\,y - 33.36\,x^6 + 2363.0\,x^5\,y^7 + 12.55\,x^5\,y^6 - 3157.0\,x^5\,y^5 - 1.75\,x^5\,y^4 + 1308.0\,x^5\,y^3 \\
& -12.29\,x^5\,y^2 - 172.8\,x^5\,y + 2.061\,x^5 + 738.3\,x^4\,y^8 - 1.204\,x^4\,y^7 - 731.3\,x^4\,y^6 + 6.304\,x^4\,y^5 + 311.2\,x^4\,y^4 \\
& +1.502\,x^4\,y^3 - 51.87\,x^4\,y^2 - 0.6299\,x^4\,y + 6.162\,x^4 + 1157.0\,x^3\,y^9 + 23.64\,x^3\,y^8 - 2075.0\,x^3\,y^7 - 22.14\,x^3\,y^6 \\
& +1282.0\,x^3\,y^5 + 6.615\,x^3\,y^4 - 346.7\,x^3\,y^3 + 1.229\,x^3\,y^2 + 33.03\,x^3\,y - 0.2878\,x^3 + 125.9\,x^2\,y^{10} + 1.089\,x^2\,y^9 \\
& -132.9\,x^2\,y^8 + 1.447\,x^2\,y^7 + 69.36\,x^2\,y^6 - 1.891\,x^2\,y^5 - 12.06\,x^2\,y^4 + 0.3594\,x^2\,y^3 + 4.222\,x^2\,y^2 + 0.06411\,x^2\,y \\
& +0.7774\,x^2 + 229.3\,x\,y^{11} + 6.496\,x\,y^{10} - 512.0\,x\,y^9 - 10.57\,x\,y^8 + 421.4\,x\,y^7 + 6.252\,x\,y^6 - 170.1\,x\,y^5 - 1.565\,x\,y^4 \\
& +32.69\,x\,y^3 + 0.1172\,x\,y^2 - 4.247\,x\,y + 0.01662\,x - 5.304\,y^{12} - 0.01646\,y^{11} + 15.82\,y^{10} + 0.1838\,y^9 - 13.83\,y^8 \\
& -0.2268\,y^7 + 6.189\,y^6 + 0.1314\,y^5 - 0.8599\,y^4 - 0.02268\,y^3 + 0.3956\,y^2 + 0.004385\,y + 0.237,
\end{aligned} \tag{A.3}
$$

$$
\begin{aligned}
C_{XY} = \; & -95.5\,x^{12} + 157.4\,x^{11}\,y + 0.4255\,x^{11} - 609.2\,x^{10}\,y^2 + 61.96\,x^{10}\,y + 221.4\,x^{10} + 956.9\,x^9\,y^3 \\
& -18.91\,x^9\,y^2 - 216.7\,x^9\,y - 0.2467\,x^9 - 639.0\,x^8\,y^4 + 13.2\,x^8\,y^3 + 985.9\,x^8\,y^2 - 92.96\,x^8\,y - 187.1\,x^8 \\
& +1941.0\,x^7\,y^5 + 6.846\,x^7\,y^4 - 1104.0\,x^7\,y^3 + 22.78\,x^7\,y^2 + 134.1\,x^7\,y - 0.1764\,x^7 - 121.9\,x^6\,y^6 + 53.21\,x^6\,y^5 \\
& +600.7\,x^6\,y^4 - 18.47\,x^6\,y^3 - 536.4\,x^6\,y^2 + 50.0\,x^6\,y + 77.4\,x^6 + 1905.0\,x^5\,y^7 + 17.89\,x^5\,y^6 - 1646.0\,x^5\,y^5 \\
& -14.57\,x^5\,y^4 + 511.3\,x^5\,y^3 - 8.21\,x^5\,y^2 - 36.35\,x^5\,y + 0.1524\,x^5 + 579.3\,x^4\,y^8 - 6.85\,x^4\,y^7 - 456.5\,x^4\,y^6 \\
& -23.18\,x^4\,y^5 - 29.54\,x^4\,y^4 + 4.619\,x^4\,y^3 + 111.3\,x^4\,y^2 - 11.44\,x^4\,y - 15.13\,x^4 + 905.8\,x^3\,y^9 + 27.55\,x^3\,y^8 \\
& -1047.0\,x^3\,y^7 - 22.82\,x^3\,y^6 + 489.3\,x^3\,y^5 + 9.067\,x^3\,y^4 - 90.65\,x^3\,y^3 + 0.7291\,x^3\,y^2 + 7.016\,x^3\,y - 0.02406\,x^3 \\
& +431.4\,x^2\,y^{10} + 23.4\,x^2\,y^9 - 749.3\,x^2\,y^8 - 12.97\,x^2\,y^7 + 408.1\,x^2\,y^6 + 6.482\,x^2\,y^5 - 81.94\,x^2\,y^4 + 0.0493\,x^2\,y^3 \\
& -2.534\,x^2\,y^2 + 1.062\,x^2\,y + 2.016\,x^2 + 177.1\,x\,y^{11} + 7.842\,x\,y^{10} - 251.0\,x\,y^9 - 9.557\,x\,y^8 + 154.2\,x\,y^7 \\
& +4.957\,x\,y^6 - 41.58\,x\,y^5 - 1.124\,x\,y^4 + 7.612\,x\,y^3 + 0.1089\,x\,y^2 + 0.3236\,x\,y + 0.01035\,x + 117.1\,y^{12} + 0.4667\,y^{11} \\
& -259.0\,y^{10} - 1.27\,y^9 + 212.2\,y^8 + 0.6678\,y^7 - 85.08\,y^6 - 0.2162\,y^5 + 16.28\,y^4 - 0.02\,y^3 - 2.059\,y^2 - 0.01685\,y - 0.0001855,
\end{aligned} \tag{A.4}
$$

$$
\begin{aligned}
C_{YX} = \; & 177.2\,x^{12} + 231.6\,x^{11}\,y - 4.85\,x^{11} + 872.5\,x^{10}\,y^2 + 1.796\,x^{10}\,y - 238.7\,x^{10} + 1222.0\,x^9\,y^3 \\
& -26.34\,x^9\,y^2 - 519.6\,x^9\,y + 9.187\,x^9 + 1634.0\,x^8\,y^4 + 13.1\,x^8\,y^3 - 911.3\,x^8\,y^2 - 3.647\,x^8\,y + 139.1\,x^8 \\
& +2386.0\,x^7\,y^5 - 7.116\,x^7\,y^4 - 2148.0\,x^7\,y^3 + 32.32\,x^7\,y^2 + 428.7\,x^7\,y - 6.448\,x^7 + 1579.0\,x^6\,y^6 - 5.404\,x^6\,y^5 \\
& -1220.0\,x^6\,y^4 - 10.06\,x^6\,y^3 + 378.6\,x^6\,y^2 + 2.45\,x^6\,y - 33.36\,x^6 + 2363.0\,x^5\,y^7 + 12.55\,x^5\,y^6 - 3157.0\,x^5\,y^5 \\
& -1.75\,x^5\,y^4 + 1308.0\,x^5\,y^3 - 12.29\,x^5\,y^2 - 172.8\,x^5\,y + 2.061\,x^5 + 738.3\,x^4\,y^8 - 1.204\,x^4\,y^7 - 731.3\,x^4\,y^6 \\
& +6.304\,x^4\,y^5 + 311.2\,x^4\,y^4 + 1.502\,x^4\,y^3 - 51.87\,x^4\,y^2 - 0.6299\,x^4\,y + 6.162\,x^4 + 1157.0\,x^3\,y^9 + 23.64\,x^3\,y^8 \\
& -2075.0\,x^3\,y^7 - 22.14\,x^3\,y^6 + 1282.0\,x^3\,y^5 + 6.615\,x^3\,y^4 - 346.7\,x^3\,y^3 + 1.229\,x^3\,y^2 + 33.03\,x^3\,y - 0.2878\,x^3 \\
& +125.9\,x^2\,y^{10} + 1.089\,x^2\,y^9 - 132.9\,x^2\,y^8 + 1.447\,x^2\,y^7 + 69.36\,x^2\,y^6 - 1.891\,x^2\,y^5 - 12.06\,x^2\,y^4 \\
& +0.3594\,x^2\,y^3 + 4.222\,x^2\,y^2 + 0.06411\,x^2\,y + 0.7774\,x^2 + 229.3\,x\,y^{11} + 6.496\,x\,y^{10} - 512.0\,x\,y^9 - 10.57\,x\,y^8 \\
& +421.4\,x\,y^7 + 6.252\,x\,y^6 - 170.1\,x\,y^5 - 1.565\,x\,y^4 + 32.69\,x\,y^3 + 0.1172\,x\,y^2 - 4.247\,x\,y + 0.01662\,x - 5.304\,y^{12} \\
& -0.01646\,y^{11} + 15.82\,y^{10} + 0.1838\,y^9 - 13.83\,y^8 - 0.2268\,y^7 + 6.189\,y^6 + 0.1314\,y^5 - 0.8599\,y^4 - 0.02268\,y^3 \\
& +0.3956\,y^2 + 0.004385\,y + 0.237;
\end{aligned} \tag{A.5}
$$

$$
\begin{aligned}
C_{YY} = \; & -95.5\,x^{12} + 157.4\,x^{11}\,y + 0.4255\,x^{11} - 609.2\,x^{10}\,y^2 + 61.96\,x^{10}\,y + 221.4\,x^{10} + 956.9\,x^9\,y^3 \\
& -18.91\,x^9\,y^2 - 216.7\,x^9\,y - 0.2467\,x^9 - 639.0\,x^8\,y^4 + 13.2\,x^8\,y^3 + 985.9\,x^8\,y^2 - 92.96\,x^8\,y - 187.1\,x^8 + 1941.0\,x^7\,y^5 \\
& +6.846\,x^7\,y^4 - 1104.0\,x^7\,y^3 + 22.78\,x^7\,y^2 + 134.1\,x^7\,y - 0.1764\,x^7 - 121.9\,x^6\,y^6 + 53.21\,x^6\,y^5 + 600.7\,x^6\,y^4 \\
& -18.47\,x^6\,y^3 - 536.4\,x^6\,y^2 + 50.0\,x^6\,y + 77.4\,x^6 + 1905.0\,x^5\,y^7 + 17.89\,x^5\,y^6 - 1646.0\,x^5\,y^5 - 14.57\,x^5\,y^4 \\
& +511.3\,x^5\,y^3 - 8.21\,x^5\,y^2 - 36.35\,x^5\,y + 0.1524\,x^5 + 579.3\,x^4\,y^8 - 6.85\,x^4\,y^7 - 456.5\,x^4\,y^6 - 23.18\,x^4\,y^5 \\
& -29.54\,x^4\,y^4 + 4.619\,x^4\,y^3 + 111.3\,x^4\,y^2 - 11.44\,x^4\,y - 15.13\,x^4 + 905.8\,x^3\,y^9 + 27.55\,x^3\,y^8 - 1047.0\,x^3\,y^7 \\
& -22.82\,x^3\,y^6 + 489.3\,x^3\,y^5 + 9.067\,x^3\,y^4 - 90.65\,x^3\,y^3 + 0.7291\,x^3\,y^2 + 7.016\,x^3\,y - 0.02406\,x^3 + 431.4\,x^2\,y^{10} \\
& +23.4\,x^2\,y^9 - 749.3\,x^2\,y^8 - 12.97\,x^2\,y^7 + 408.1\,x^2\,y^6 + 6.482\,x^2\,y^5 - 81.94\,x^2\,y^4 + 0.0493\,x^2\,y^3 - 2.534\,x^2\,y^2 \\
& +1.062\,x^2\,y + 2.016\,x^2 + 177.1\,x\,y^{11} + 7.842\,x\,y^{10} - 251.0\,x\,y^9 - 9.557\,x\,y^8 + 154.2\,x\,y^7 + 4.957\,x\,y^6 - 41.58\,x\,y^5 \\
& -1.124\,x\,y^4 + 7.612\,x\,y^3 + 0.1089\,x\,y^2 + 0.3236\,x\,y + 0.01035\,x + 117.1\,y^{12} + 0.4667\,y^{11} - 259.0\,y^{10} - 1.27\,y^9 \\
& +212.2\,y^8 + 0.6678\,y^7 - 85.08\,y^6 - 0.2162\,y^5 + 16.28\,y^4 - 0.02\,y^3 - 2.059\,y^2 - 0.01685\,y - 0.0001855,
\end{aligned}
\tag{A.6}
$$

References

[1] Tiwari R. Rotor systems: analysis and identification. CRC Press; 2017.
[2] Reynolds O. On the theory of lubrication and its application to Mr. Beauchamp tower's experiments, including an experimental determination of the viscosity of olive oil. Philos Trans R Soc Lond 1886;177:157–234. ⟨http://www.jstor.org/stable/109480⟩.
[3] Ruggiero A, Senatore A. Approximate closed-form solution for the dynamical analysis of short bearings with couple stress fluid. Lubr Sci 2007;19(4):247–67. https://doi.org/10.1002/ls.47.
[4] Chiang HL, Lin JR, Hsu CH, Chang YP. Linear stability analysis of a rough short journal bearing lubricated with non-Newtonian fluids. Tribol Lett 2004;17(4):867–77. https://doi.org/10.1007/s11249-004-8095-8 [cited By:17 Export Date: 22 December 2020].
[5] Liao WH, Lu RF, Chien RD, Lin JR. Linear stability analysis of long journal bearings: couple stress fluid model. Ind Lubr Tribol 2005;57(1):21–7. https://doi.org/10.1108/00368790510575950 [cited By:7 Export Date: 22 December 2020].
[6] Amamou A, Chouchane M. Nonlinear stability analysis of long hydrodynamic journal bearings using numerical continuation. Mech Mach Theory 2014;72:17–24. https://doi.org/10.1016/j.mechmachtheory.2013.10.002.
[7] DuBois GB, Ocvirk FW. Analytical derivation and experimental evaluation of short-bearing approximation for full journal bearing. Report 1953. ⟨https://digital.library.unt.edu/ark:/67531/metadc60530/⟩.
[8] Ocvirk FW. Short-bearing approximation for full journal bearings. Rep Citeseer 1952. ⟨https://digital.library.unt.edu/ark:/67531/metadc56460/⟩.
[9] Sommerfeld A. The hydrodynamic theory of lubrication friction. Z für Math und Phys 1904;50(1–2):97–155.
[10] Elrod H, Burgdorfer A. Refinements of the Theory of the Infinitely-long49. Office of Naval Research, Department of the Navy; 1960. p. 93.
[11] Sfyris D, Chasalevris A. An exact analytical solution of the Reynolds equation for the finite journal bearing lubrication. Tribol Int 2012;55:46–58.
[12] Vignolo GG, Barilá DO, Quinzani LM. Approximate analytical solution to reynolds equation for finite length journal bearings. Tribol Int 2011;44(10):1089–99. https://doi.org/10.1016/j.triboint.2011.03.020.
[13] Bastani Y, de Queiroz M. A new analytic approximation for the hydrodynamic forces in finite-length journal bearings. J Tribol 2009;132(1). https://doi.org/10.1115/1.4000389.
[14] Nicoletti R. Comparison between a meshless method and the finite difference method for solving the reynolds equation in finite bearings. J Tribol 2013;135(4).
[15] Gnanadoss AA, Osborne MR. The numerical solution of Reynolds 'equation for a journal bearing. Q J Mech Appl Math 1964;17(2):241–6.
[16] Gero LR, Ettles CMMcC. An evaluation of finite difference and finite element methods for the solution of the Reynolds equation. ASLE Trans 1986;29(2):166–72.
[17] Ettles CM, Anderson HG. The use of higher order finite element methods for the solution of Reynolds' equation. Tribol Trans 1990;33(2):163–70.
[18] Lund JW. The stability of an elastic rotor in journal bearings with flexible, damped supports. J Appl Mech 1965;32(4):911–20. https://doi.org/10.1115/1.3627335.
[19] Lund JW. Stability and damped critical speeds of a flexible rotor in fluid-film bearings. J Eng Ind 1974;96(2):509–17. https://doi.org/10.1115/1.3438358.
[20] Peng J-P, Carpino M. Calculation of stiffness and damping coefficients for elastically supported gas foil bearings. J Tribol 1993;115(1):20–7. https://doi.org/10.1115/1.2920982.
[21] Dyk v, Rendl J, Byrtus M, Smolík L. Dynamic coefficients and stability analysis of finite-length journal bearings considering approximate analytical solutions of the reynolds equation. Tribol Int 2019;130:229–44. https://doi.org/10.1016/j.triboint.2018.09.011.
[22] Miraskari M, Hemmati F, Gadala MS. Nonlinear dynamics of flexible rotors supported on journal bearings–Part i: analytical bearing model. J Tribol 2018;140(2). https://doi.org/10.1115/1.4037730.
[23] Miraskari M, Hemmati F, Gadala MS. Nonlinear dynamics of flexible rotors supported on journal bearings–Part ii: numerical bearing model. J Tribol 2018;140(2):021705. https://doi.org/10.1115/1.4037731.
[24] Muszynska A. Stability of whirl and whip in rotor/bearing systems. J Sound Vib 1988;127(1):49–64. https://doi.org/10.1016/0022-460X(88)90349-5.
[25] Deepak JC, Noah ST. Experimental verification of subcritical whirl bifurcation of a rotor supported on a fluid film bearing. J Tribol 1998;120(3):605–9. https://doi.org/10.1115/1.2834593.
[26] Weimin W, Lihua Y, Tiejun W, Lie Y. Nonlinear dynamic coefficients prediction of journal bearings using partial derivative method. Proc Inst Mech Eng Part J: J Eng Tribol 2012;226(4):328–39. https://doi.org/10.1177/1350650111431526.
[27] Sayed H, El-Sayed TA. Nonlinear dynamics and bifurcation analysis of journal bearings based on second order stiffness and damping coefficients. Int J Non-Linear Mech 2022;142:103972. https://doi.org/10.1016/j.ijnonlinmec.2022.103972. ⟨https://www.sciencedirect.com/science/article/pii/S0020746222000439⟩.
[28] Meruane V, Pascual R. Identification of nonlinear dynamic coefficients in plain journal bearings. Tribol Int 2008;41(8):743–54. https://doi.org/10.1016/j.triboint.2008.01.002.
[29] Elsayed T, Sayed H. Bifurcation analysis of rotor/bearing system using third-order journal bearing stiffness and damping coefficients. Nonlinear Dyn Access via Springe Agreem 2021. https://doi.org/10.1007/s11071-021-06965-4.
[30] Fedor JV. Half Sommerfeld approximation for finite journal bearings. J Basic Eng 1963;85(3):435–8. https://doi.org/10.1115/1.3656638.
[31] Fedor JV. A Sommerfeld solution for finite bearings with circumferential grooves. J Basic Eng 1960;82(2):321–6. https://doi.org/10.1115/1.3662589.
[32] Barrett LE, Allaire PE, Gunter EJ. A finite length bearing correction factor for short bearing theory. J Lubr Technol 1980;102(3):283–7. https://doi.org/10.1115/1.3251508.
[33] Rahmanzadeh-Asl M, Ettles CMM. Discussion: "a finite length bearing correction factor for short bearing theory" (Barrett, l. E., Allaire, P. E., and Gunter, E. J., 1980, ASME J. Lubr. Technol., 102, pp. 283–287). J Lubr Technol 1980;102(3):287–8. https://doi.org/10.1115/1.3251509.
[34] Hirani H, Athre K, Biswas S. Dynamically loaded finite length journal bearings: analytical method of solution. J Tribol 1999;121(4):844–52. https://doi.org/10.1115/1.2834144.
[35] Falkenhagen GL, Gunter EJ, Schuller FT. Stability and transient motion of a vertical three-lobe bearing system. J Eng Ind 1972;94(2):665–76. https://doi.org/10.1115/1.3428225.
[36] WangW, Zhang Z. Nonlinear oil film force database, vol. 14; 1993, p. 299–305.
[37] Chen Z, Jiao Y, Xia S, Huang W, Zhang Z. An efficient calculation method of nonlinear fluid film forces in journal bearing. Tribol Trans 2002;45(3):324–9. https://doi.org/10.1080/10402000208982556.
[38] Chasalevris A, Louis J-C. Evaluation of transient response of turbochargers and turbines using database method for the nonlinear forces of journal bearings. Lubricants 2019;7(9):78. ⟨https://www.mdpi.com/2075-4442/7/9/78⟩.
[39] Smolík L, Rendl J, Dyk u, Polach P, Hajžman M. Threshold stability curves for a nonlinear rotor-bearing system. J Sound Vib 2019;442:698–713. https://doi.org/10.1016/j.jsv.2018.10.042.
[40] Chasalevris A. Stability and hopf bifurcations in rotor-bearing-foundation systems of turbines and generators. Tribol Int 2020;145:106154. https://doi.org/10.1016/j.triboint.2019.106154.
[41] Wang JK, Khonsari MM. Bifurcation analysis of a flexible rotor supported by two fluid-film journal bearings. J Tribol 2006;128(3):594–603. https://doi.org/10.1115/1.2197842.
[42] Wang JK, Khonsari MM. Application of hopf bifurcation theory to rotor-bearing systems with consideration of turbulent effects. Tribol Int 2006;39(7):701–14. https://doi.org/10.1016/j.triboint.2005.07.031. ⟨https://www.sciencedirect.com/science/article/pii/S0301679X05002070⟩.
[43] Wang JK, Khonsari MM. Influence of inlet oil temperature on the instability threshold of rotor-bearing systems. J Tribol 2005;128(2):319–26. https://doi.org/10.1115/1.2162920.
[44] Chouchane M, Amamou A. Bifurcation of limit cycles in fluid film bearings. Int J Non-Linear Mech 2011;46(9):1258–64. https://doi.org/10.1016/j.ijnonlinmec.2011.06.005.
[45] Dhooge A, Govaerts W, Kuznetsov YA. Matcont: a matlab package for numerical bifurcation analysis of odes. ACM Trans Math Softw (TOMS) 2003;29(2):141–64.